Structure-Function Relationship of Surface N-glycans and Enzyme Active Site Proficiency: A Kinetic and Hydrogen-Deuterium Exchange Investigation of *Mo*LOX

by

Chris Whittington

July 2021

Director of Thesis: Adam R. Offenbacher

Major Department: Chemistry

A ‘unique’ enzyme has emerged within the lipoxygenase (LOX) family. This manganese containing enzyme comes from the pathogen *Magnaporthe oryzae* and termed *Mo*LOX. *Mo*LOX is secreted at the onset of pathogenesis when the rice blast fungus infects a rice plant that accounts for the loss of 1/3 of the world’s rice crops. *Mo*LOX has many different features when compared to the rest of the LOX family, including the presence of eight N-linked glycans at the surface of the enzyme, which is the focus of this Thesis. We used multiple methods to remove the glycans from the surface including treatment with PNGase F and Endo H as well as asparagine to glutamine site directed mutagenesis. Steady state kinetics was employed to determine the impact of glycan removal on first- and second-order kinetic parameters for protio substrates as well as using a deuterated substrate to help determine the impact on the kinetic isotope effects, useful probes in the case of LOX C-H activation. In addition, hydrogen-deuterium exchange mass spectrometry (HDX-MS) was used to determine the effect of glycan removal on regional protein flexibility. From these studies, we have identified regions of the protein that account for altered catalytic proficiency and substrate selectivity that depends upon the deglycosylation method deployed.

Structure-Function Relationship of Surface N-glycans and Enzyme Active Site Proficiency: A Kinetic and Hydrogen-Deuterium Exchange Investigation of *Mo*LOX

A Thesis

Presented to the Faculty of the Department of Chemistry

East Carolina University

In Partial Fulfillment of the Requirements for the Degree

Master of Science in Chemistry

by

Chris Whittington

July 2021

Structure-Function Relationship of Surface N-glycans and Enzyme Active Site Proficiency: A Kinetic and Hydrogen-Deuterium Exchange Investigation of *Mo*LOX

By

Chris Whittington

APPROVED BY:

DIRECTOR OF THESIS: _____

Adam R. Offenbacher, Ph.D.

COMMITTEE MEMBER: _____

William E. Allen, Ph.D.

COMMITTEE MEMBER:_____

Sambuddah Banerjee, Ph.D.

COMMITTEE MEMBER:_____

Jun-yong Choe, Ph.D.

COMMITTEE MEMBER:_____

Patrick Horn, Ph.D.

CHAIR OF THE

DEPARTMENT OF CHEMISTRY:_____

Andrew T. Morehead, Jr., Ph.D.

DEAN OF THE

GRADUATE SCHOOL: _____

Paul Gemperline, Ph.D.

ACKNOWLEDGEMENTS

I would first like to thank my thesis advisor, Dr. Adam Offenbacher, he has taught me everything I know and has made me into the chemist that I am now. He taught me the questions to ask as well as how to look for the right answers.

Next, I would like to thank the Chemistry Department at ECU, as well as the entire Offenbacher Lab. We have stood by each other and with the help of Kristin Tyson, we built the lab culture that will endure for many years to come.

Also, I want to thank my family as well as my family of friends that I have made over the years at ECU. I want to thank Josie, Megan, and Abby for keeping me sane as we went through the years here together and always giving me the best advice and even better reasons to laugh.

Lastly, I want to thank my fiancée Landri, without her support and the drive for the life we want I don’t think I could’ve gotten through the majority of my hurdles. Thanks for always standing by me as I read through multiple papers and made many presentations, I couldn’t have done it without you.

TABLE OF CONTENTS

LIST OF TABLES

CHAPTER 2

APPENDIX A

LIST OF FIGURES

CHAPTER 1

CHAPTER 2

APPENDIX A

I. Introduction to Manganese Lipoxygenase

Manganese Lipoxygenase: Emergence of an 'unusual' lipoxygenase

Fungal lipoxygenases (LOXs) were first discovered in the late 1990's/early 2000's and are considered to be 'unusual' compared to the typical iron lipoxygenases for three reasons. First, they generate products that are quite different than the ones from the mammalian and plant LOXs: a unique bis-allylic hydroperoxide (11-HPODE) opposed to the conjugated hydroperoxides (9,13-HPODE) that are produced by the mammalian and plant LOXs (**Figure 1.1**).[1] Second, the fungal LOXs also contain a different metal, manganese, as their reactive cofactor.[2] Other than fungal enzymes, all lipoxygenases use iron as the catalytic cofactor. It has been shown that the substitution of a Fe center for Mn, in either animal or plant LOXs, renders the enzyme inactive.[3] The physical basis would likely entail the unique positioning of second shell ligands to the metal center.[4] Third, and the focus of this thesis is the presence of N-linked glycans that decorate the outside of the protein.[2]

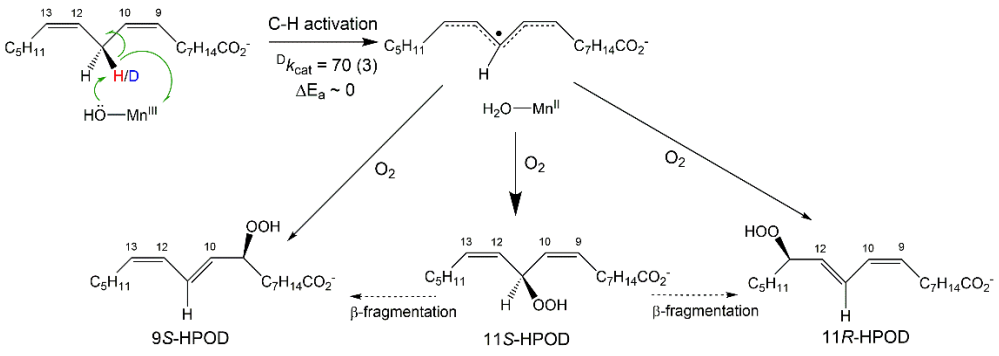

Figure 1.1: *Reaction of Mo*LOX *with linoleic acid (LA) proceeds through an initial and rate-limiting C-H activation step*

As a model enzyme, we chose the lipoxygenase produced by the rice blast fungus *Magnaporthe oryzae* (also known as *Magnaporthe grisea*). *M. oryzae* is currently considered the most destructive plant pathogen and is responsible for the loss of 10-30% of the world's total rice harvest.[5] This has caused it to be considered one of the top ten most deadly and important fungal pathogens in molecular biology. Its lipoxygenase, which is termed *Mo*LOX, is secreted from the fungus at the onset of pathogenesis. The latter was demonstrated by a research group at the Department of Pharmaceutical Biosciences at Uppsala University reporting that the mRNA expression levels of *Mo*LOX are correlated with the formation of the appressorium, which is the infectious part of the fungus (**Figure 1.2**).[2] Negligible mRNA levels of *Mo*LOX were produced during the vegetative (non-infectious) stage (i.e. mycelium). From these results, *Mo*LOX has been implicated in pathogenesis and considered a potential molecular target for inhibition of rice blast disease. However, the role of its unique bis-allylic products on plant pathogenesis and the rice plant is currently unknown and don't appear to have a role in cell signaling like their LOX counterparts.

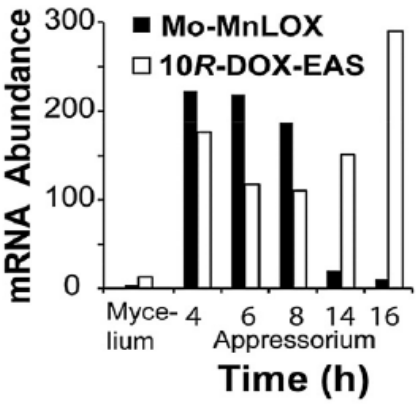

Figure 1.2: *Levels of transcripts of Mo-Mn*LOX *and 10R-DOX-EAS (10R-dioxygenase-epoxy alcohol synthase) in mycelium (vegetative part of the fungus) and during formation of appressorium. (Reproduced from reference 2)*

*Structural Aspects of Mo*LOX

The role of *Mo*LOX in pathogenesis could be addressed through the development of *Mo*LOX selective inhibitors. As an important first step towards *Mo*LOX inhibitor design, the crystal structure of *Mo*LOX has been solved to 2.0Å resolution.[5] However, to promote crystallization the glycans were processed with the enzyme, endoglycosidase H (EndoH), which cleaves the native, complex glycan structures leaving a single N-acetylglucosamine (GlcNAc) remaining on the asparagine (Asn) – (**Figure 1.3**). Despite the wealth of information afforded by the crystal structure, it is not well understood how changing the glycan pattern may alter the global and/or active site structure. This information is anticipated to serve as a foundation for structure-based guidance in the design and development of *Mo*LOX specific inhibitors.

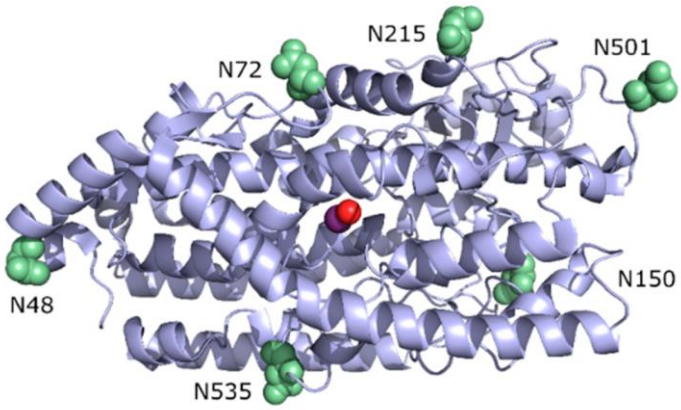

Figure 1.3: *X-ray model (2.0 Å; PDB: 5FNO) determined for endoglycosidase H treated Mo*LOX. *The catalytic cofactor, Mn^{2+}-OH_2 (reduced state), are the colored purple and red spheres, respectively. Asn residues that are predicted to be glycosylated are shown as green spheres. There are two additional Asn residues (N18 and N28) predicted to be glycosylated, but their electron density was not resolved.*

Metal Coordination Sphere and Adjustment of Redox Potential

The catalytic metal of *Mo*LOX is Mn^{2+} and has been shown to coordinate with His-294, His-289, His-469, Asn-473, Val-605, and a H_2O molecule. This is similar to 8R-LOX but doesn't superimpose as well as 8R-LOX, sLOX-1, and 15S-LOX.

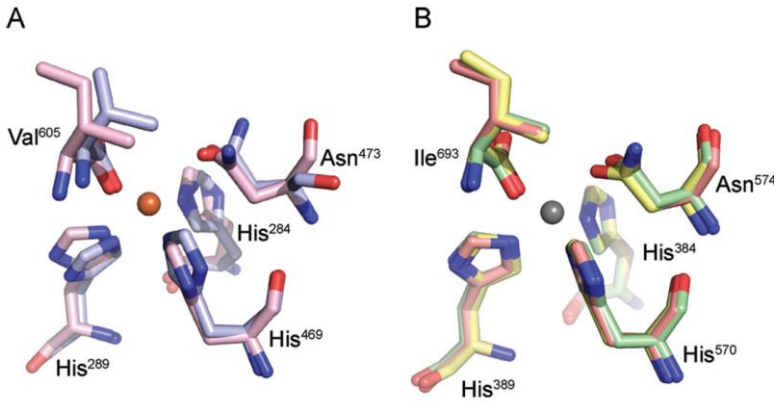

Figure 1.4: *The catalytic manganese (orange sphere) of Mn-Mo*LOX *(purple) is coordinated in a distorted octahedron. The active site of 8R*-LOX *(PDB 4QWT, pink) is overlaid on top with a r.m.s deviation of 0.57Å. The largest difference between the two is seen in the Asn residues and the C-terminal Val/Ile residues. In panel B three different Fe*LOX *[8R*-LOX *(PDB 4QWT, red), s*LOX-*1 (PDB 1YGE, green), and 15S*-LOX *of P.aeruginoas (PDB 4G32, yellow)] are overlaid around the iron catalytic center (grey sphere) with an r.m.s deviation between 0.23 and 0.29Å.(Reproduced from reference 5)*

Interest has been placed on the weak axial ligand Asn-473, which crystal structures have shown to be positioned on a short loop in *Mo*LOX while the orthologous asparagine side chain is located in an a-helix in iron LOXs (**Figure 1.4**). The placement of this Asn on a loop instead of a helix may be due to the presence of Pro-447 which is conserved in all *Mo*LOX but not present in iron LOXs. Since proline is a known helix breaker this could be the reason that Asn-473 on the loop is able to get near the catalytic metal. The flexibility that is provided by the short loop may

lead to a Jahn-Teller distortion of the octahedron coordination of Mn^{2+} during oxidation from Mn^{2+} to Mn^{3+}.[5] Strategic site-directed mutagenesis investigations are needed to validate this hypothesis.

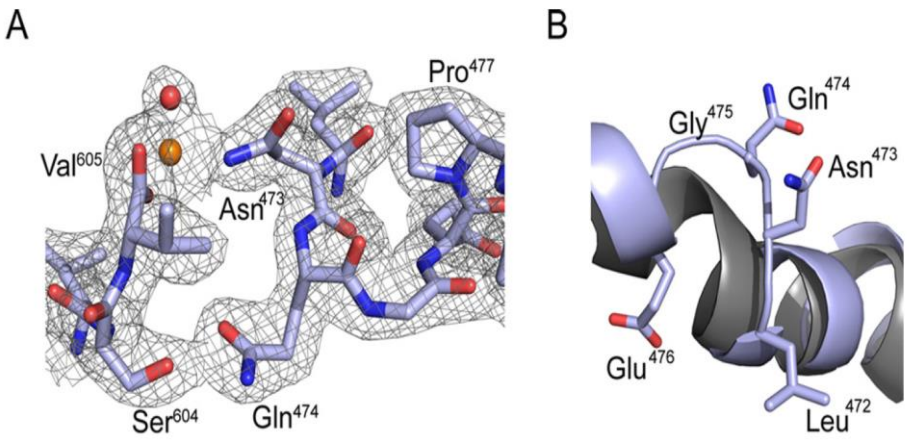

Figure 1.5: *(A) shows the electron density map of a loop in an a-helix near the active site. (B) shows a ribbon model of the same loop and how it sits between two parts of the same α-helix. The helix is shown broken in Mn-Mo*LOX *(purple) but complete in (grey). (Reproduced from reference 5)*

The overall flexibility and movement of the coordination sphere as well as the hydrogen bond to the catalytic center is what likely accounts for the redox potential adjustment. Fe^{3+}/Fe^{2+} has a standard reduction potential of ~0.75V while Mn^{3+}/Mn^{2+} has a standard reduction potential of ~1.5V. Both catalytic centers are both expected to be 0.6-0.7V in the enzyme as they catalyze the same reaction.[6] For iron LOXs this is just a minor adjustment, but it is an impressive ~1.0V difference for *Mo*LOX which shows how crucial the flexibility and hydrogen bonding might need to be to harness the proper reduction potentials for catalysis.

Active Site and the Oxygenation Mechanism

The crystal structure of *Mo*LOX revealed a U-shaped substrate channel similar to that of 8R-LOX and iron LOXs and has been shown to be solvent exposed with spacious 'pockets' that are close to the presumed position of the assumed pentadiene radical for hydrogen abstraction and oxygenation.[5] It is not clear if the substrate binds and then oxygen or vice versa. The depth of the channel is most likely controlled by Phe-342 at the Sloane determinant, while Phe-332 and Phe-526 may directly influence the stereospecific oxygenation of the substrate (**Figure 1.6**)

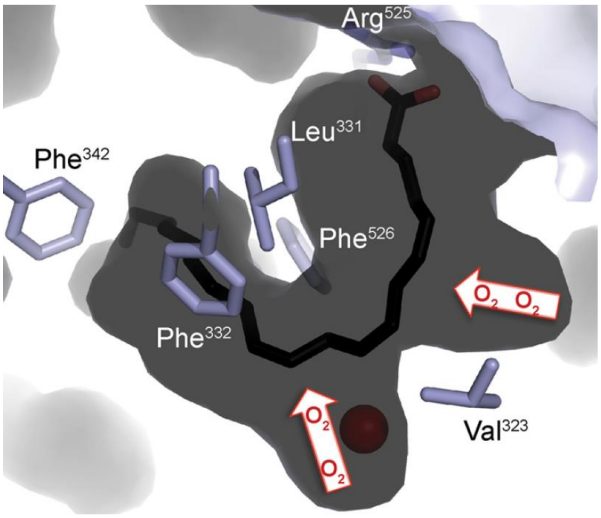

Figure 1.6: *Cartoon representation of the active site of Mn-Mo*LOX *showing the surrounding residues and possible O_2 insertion to the substrate. Phe-342 likely controls the depth of the substrate channel while F332/F526 may influence the stereospecificity of oxygenation. (Reproduced from reference 5)*

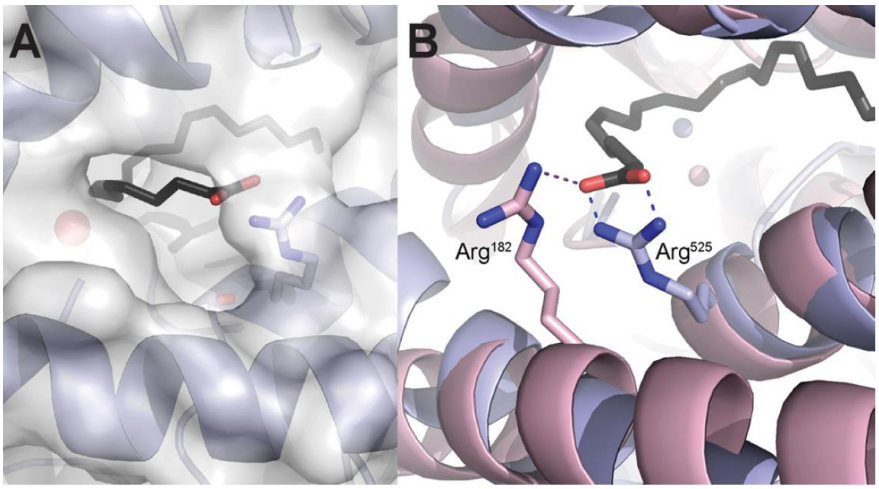

Figure 1.7: *A cartoon representation of the crystal structure of Mn-Mo*LOX *(purple) and 8R*-LOX *(pink). (A) shows the entrance of the substrate channel at the surface of the enzyme showing that the channel is solvent exposed. (B) shows the active sites of the two enzymes overlain and shows the two arginine (Arg-182 and Arg-525) which may tether the substrate into the channel itself. (Reproduced from reference 5)*

Phe-332 may tether the substrate in the channel along with Arg-525, as well as shield the opposite side of the substrate from oxygenation. Arg-525 is suggested to help tether the substrate into the substrate channel and is similar to Arg-182 in 8R-LOX (**Figure 1.7B**)

*pH Dependence of Mo*LOX *Reaction*

From previous kinetic analysis from our lab[7], the k_{cat} for *Mo*LOX with natural substrate, linoleic acid (H-LA), was found to be 2.5±0.2 s^{-1}, which is consistent with the previously reported value of 2.7±0.3 s^{-1}.[2] Additionally, it was shown that the k_{cat} was constant over a pH value range of 7-9 which indicated that the reaction is pH independent. When compared to H-LA, the deuterated substrate (D-LA) was nearly 2 orders of magnitude smaller but was still able to maintain its pH independence (Figure 8A). The combination of these measurements allowed an overall first-order kinetic isotope effect, $^{D}k_{cat}$, of 60-80 to arise (**Figure 1.8A**). This value is twice of the reported value of 40 at pH 9 for the monodeuterated 11S-D-LA[2] and much larger than the reported

value of 20 for the take all fungus *G.graminis*[8], though comparable to that of the model plant enzyme, SLO ($^{D}k_{cat}$ = 60-80). Extending the analysis to the second-order rate constant (k_{cat}/K_M) shows a modest effect on H-LA and a lack of pH dependence on D-LA (**Figure 1.8B**). At pH 7, the second-order kinetic isotope effect, $^{D}k_{cat}/K_M$, is approximately half of that at the pH range of 8-9 and at elevated pH values the $^{D}k_{cat}/K_M$ is seen to match or slightly exceed $^{D}k_{cat}$. This data supported the idea that there was no pKa for a protein residue(s) that might affect substrate binding. This apparent lack of pH dependence for k_{cat}, k_{cat}/K_M, and the large value for $^{D}k_{cat}/K_M$ along with the reduced turnover number for *Mo*LOX led to the conclusion that the initial (and irreversible) C-H activation step is the dominant rate limiting step of catalysis and there is little contribution from the substrate on and off microscopic rates.

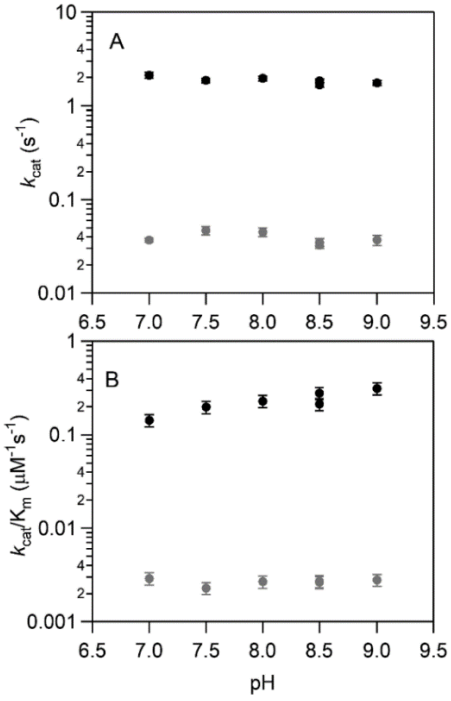

Figure 1.8: *Plot of the pH dependence of (A) k_{cat} and (B) k_{cat}/K_M for native Mo*LOX. *Data for H-LA are shown as black circles, and the data for D-LA are shown as grey circles. The pH 8.5 experiment was reproduced with both 0.1 M Tris-HCl and 0.1 M borate to demonstrate the lack of dependence on the nature of the buffer. (Reproduced from reference 7)*

*Temperature Dependence of Mo*LOX *Kinetics*

The temperature dependence of k_{cat} was also found to be 9.7±0.5 kcal/mol over this temperature (10-30 °C) range. This value is similar to *Gg*LOX at E_a ~ 10-11 kcal/mol[9], but much higher than the reported value for SLO which is around 2 kcal/mol (**Figure 1.9A, black trace**). The k_{cat} was shown to have considerable temperature dependence while the $^{D}k_{cat}$ is nearly temperature independent [$\Delta E_a = E_a(D) - E_a(H) = -1.1\pm0.5$ kcal/mol for *Mo*LOX and $\Delta E_a = 1.2 \pm .2$ kcal/mol for SLO] (**Figure 1.9B**). Even though the ΔE_a for the native *Mo*LOX is slightly negative the results in Figure 9 strongly support a nonclassical, full tunneling mechanism for the reaction with LA.[7] In addition to the large $^{D}k_{cat}$, the effect on the second-order rate constant, $^{D}k_{cat}/K_M$, is large (≥ 30) and temperature independent which supported the conclusion that the rate of reaction for *Mo*LOX with LA is completely dominated by the C-H cleavage step.

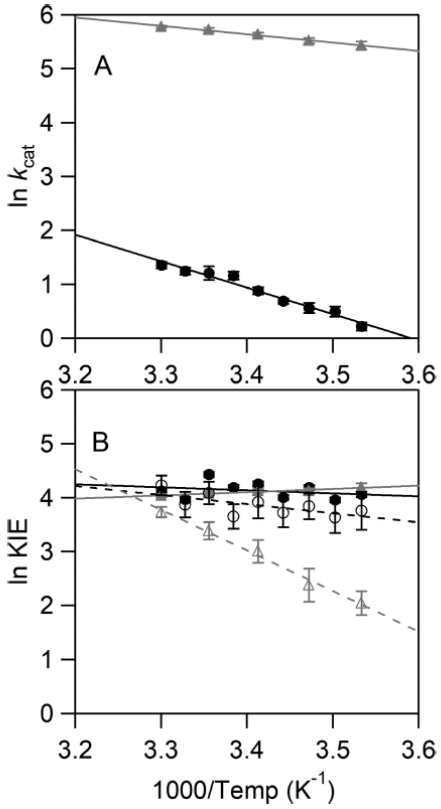

Figure 1.9: *Plot of the temperature dependence of (A) k_{cat} and (B) kinetic isotope effects (KIEs) for native MoLOX (black circles) and SLO (grey triangles). In panel B the temperature dependence of $^{D}k_{cat}$ (filled symbols) and $^{D}k_{cat}/K_M$ (empty symbols) is presented. These rate constants were measured in 0.1 M borate (pH 9.0). (Reproduced from reference 7)*

Significance of a Temperature-Independent $^{D}k_{cat}/K_M$ for MoLOX

There remains a limited structural basis for the substrate binding and acquisition for these manganese lipoxygenases from pathogenic fungi which restricts design strategies for structure-based inhibitors. However, both *Gg*LOX and *Mo*LOX do share the lack of the C2-like N-terminal PLAT domain that it conserved in higher eukaryotes.[10] The PLAT domains have been implicated in Ca^{2+}-mediated membrane association and allosteric regulation of substrate acquisition.[11,12] For example, oleic acid and oleyl sulfate have been shown to associate at the N-terminal PLAT domain and eliminate the partial rate-determining step of substrate binding at low temperatures observed

for plant and human lipoxygenases.[13–15] $^{D}k_{cat}/K_M$ serves as a kinetic reporter for effector regulation of catalysis, and $^{D}k_{cat}/K_M$ values for SLO and human 15-LOX are significantly lower than $^{D}k_{cat}$ at temperatures lower than 20 °C, but with the addition of effector, the $^{D}k_{cat}/K_M$ values increase to match the enormous value of $^{D}k_{cat}$. Conversely, the temperature analysis for *Mo*LOX kinetics shows that $^{D}k_{cat}/K_M$ is nearly equivalent to $^{D}k_{cat}$ at all temperatures including 10 °C. These kinetic results along with the evolutionary absence of the PLAT domain, further implicated a role for the PLAT domain in effector (or substrate)-induced regulation of substrate binding in LOXs from higher eukaryotes. Importantly, these data support that *Mo*LOX is not allosterically controlled.

Effect of N-linked Glycosylation on Enzyme Kinetics

In our lab's initial kinetic reporting of *Mo*LOX, the enzyme was treated with a deglycosylating enzyme, PNGase F that cleaves the full glycan structure from the N-linked asparagine residue and converts it to aspartic acid. The resulting temperature dependence (for H-LA) of this PNG-treated *Mo*LOX [$E_a(H)$ = 10 kcal/mol] is nearly identical to *Mo*LOX. While the E_a for hydrogen transfer remained the same, there was a significant difference between the temperature dependence of the kinetic isotope effect, ΔE_a, which supported the conclusion that there is an increase in E_a for deuterium transfer, $E_a(D)$. The difference between native and PNG-treated *Mo*LOX ΔE_a values [$\Delta\Delta E_a = \Delta E_a$(deglycosylated) $-\Delta E_a$(native)] is ~1.7±0.8 kcal/mol which supports a disproportionate increase to $E_a(D)$ with respect to $E_a(H)$ when treated with PNGase F (**Figure 1.10**). This result is significant because the magnitude of ΔE_a for enzymatic C-H activation has emerged as a valuable kinetic reporter on the degree of optimization in the tunneling ready state (TRS) and is a marker for the efficiency of enzyme catalyzed C-H activation. So, the data showed that there is evidence for an impaired positioning of the substrate in the active

site when *Mo*LOX is treated with PNGaseF which leads to a decreased in effectiveness in the wave overlap in the TRS.

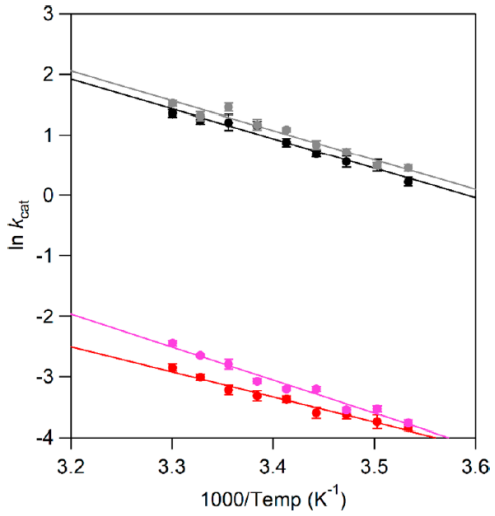

Figure 1.10: *Arrhenius plots for reactions of MoLOX with linoleic acid in 0.1 M borate (pH 9.0). The data are for (black) native MoLOX with H-LA, (grey) PNG1P-treated MoLOX with H-LA, (red) native MoLOX with D-LA, and (pink) PNG1P-treated MoLOX with D-LA. (Reproduced from reference 7)*

Impact of N-linked Glycosylations on C-H Activation

N-linked glycosylations have the potential to strongly influence the structure, stability, and folding of proteins.[16] The innate nature of the rate limiting C-H activation step of *Mo*LOX catalysis provides a unique opportunity to resolve the effects of protein modifications on the entire shape of the catalytic barrier.[17,18] Having established that $^{D}k_{cat}$ is large and independent of both pH and temperature for native *Mo*LOX, the surface glycans on the catalytic efficiency of C-H activation. Typically, EndoH is used to perform the deglycosylation but in this case PNGaseF was used. PNGaseF was expected to lead to a greater charge in water disordering at the surface. The first layers of the hydration shell at the protein surface are expected to play a significant role in

functionally relevant protein motions by so called “solvent slaving”.[19] Surprisingly, the enthalpy barriers for hydrogen transfer from the H-LA substrate for the native and the deglycosylated samples were identical [~ 10 kcal/mol]. Typically, site-directed mutations at critical residues for C-H activation are often characterized by altered activation energies with increased ΔE_a values. However, there is a functionally altering mutant of SLO, I553A, that exhibits an activation energy that is comparable to the wild-type enzyme.[20]

Despite having similar E_a values, the I553A causes a significant impairment of substrate positioning in the ground state, as measured by electron-nuclear double resonance (ENDOR) spectroscopy.[21] The impaired positioning is then propagated to the TRS as determined by an increased ΔE_a.[20,22] One of the most important things to emerge from the kinetic study of PNG1P was the increase in enthalpic barrier for deuterium transfer $E_a(D)$ which in turn shows an elevated ΔE_a. From a non-adiabatic theoretical model for the rate expression of C-H activation[17,20,22–27] a disproportionate increase in $E_a(D)$ as related to $E_a(H)$ are attributed to the impairment of the TRS, resulting in an increase in the distance between the donor and acceptor which leads to a decreased probability for hydrogenic wave function overlap. Since the wave function of deuterium is less diffuse, any type of elongation in the equilibrium donor-acceptor distance requires enhanced thermal sampling of the donor and acceptor to broaden the deuterium potential, leading to a recovery of the probability for wave function overlap. This increase in thermal motions leads to a larger $E_a(D)$ in relation to $E_a(H)$ which in turn leads to an increase in ΔE_a. The link between manipulations at the surface (the closest Asn residue is ≥16Å away from the active site residues) and the buried active site is a result of the thermal motions that are expected to be the origins of the empirical E_a barrier for enzyme C-H activation reactions.[18]

SDS-PAGE shows that the glycans add at least 60% to the theoretical mass of *Mo*LOX to the surface of the protein. MnLOX from both native fungal sources and recombinant expressions *P. pastoris*[2,28] exhibit heterogeneous gel migration patterns consistent with masses of 110-140 kDa, even though their theoretical masses based on the primary sequence are in the range of 67-75 kDa. So, the idea is favored that the increase in ΔE_a from PNGaseF treated *Mo*LOX comes from the loss of the surface glycans.

There are eight NxS/T motifs, seven are predicted sites for N-linked glycosylation, based on prediction software which searches for NxS/T primary sequence motif, where (x) can only be certain amino acid residues and has an impact on the actual formation of glycans at those postitions.[7] Importantly, our group has shown that processing these glycans with a novel PNGaseF enzyme, PNG1P, causes an impact to the kinetic parameters that implicate a perturbation of the active site structure when glycans are removed.[8] In general, PNGases transform the Asn→Asp (**see Figure 1.11**). Because our lab observed a change in kinetic parameters upon PNG1P treatment, the question emerges: are the kinetic parameters sensitive to removal of the glycans and/or change in charge distribution at the surface caused by N→Q? In addition to this question, our PNG1P treatment of *Mo*LOX is different from that of the Endo H treatment used to determine the X-ray structure. The focus of this thesis is to fill in the gaps in knowledge and provide a structural fingerprint of the effects of altered glycosylation manipulation on the local and global protein structure.

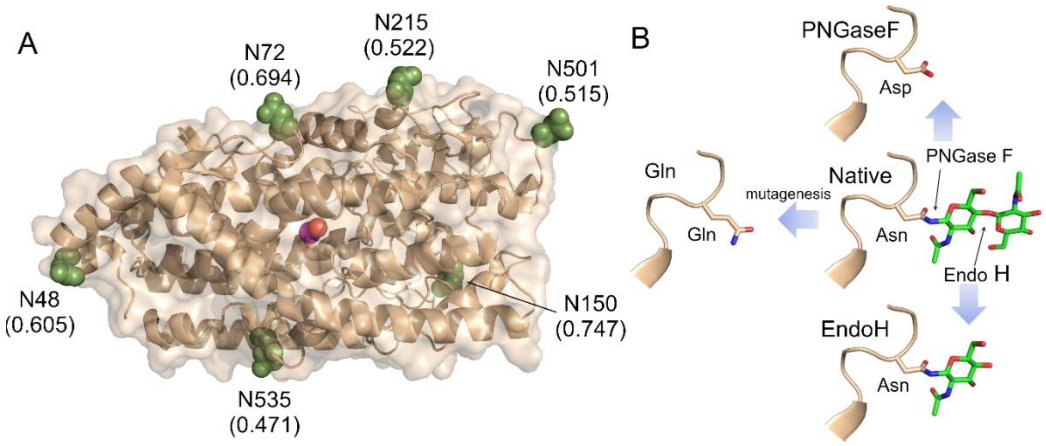

Figure 1.11: *Structure of MoLOX with the putative N-linked glycosylation sites shown as spheres (A). The potentials for the glycosylation sites are shown in parentheses. The catalytic cofactor, Mn^{2+}-OH_2, are represented as purple and red spheres, respectively. (B) Diagram illustrating the methods for N-linked glycan processing (blue arrows). The green sticks represent N-GlcNac residues and the full glycan structures have been removed for clarity. For 'GLN' MoLOX variant, all eight asparagine sidechains as predicted N-linked glycosylation sites were mutated to glutamine.*

References

(1) Haeggström, J. Z.; Funk, C. D. Lipoxygenase and Leukotriene Pathways: Biochemistry, Biology, and Roles in Disease. *Chemical Reviews*. 2011. https://doi.org/10.1021/cr200246d.

(2) Wennman, A.; Jernerén, F.; Magnuson, A.; Oliw, E. H. Expression and Characterization of Manganese Lipoxygenase of the Rice Blast Fungus Reveals Prominent Sequential Lipoxygenation of α-Linolenic Acid. *Arch. Biochem. Biophys.* 2015, *583*. https://doi.org/10.1016/j.abb.2015.07.014.

(3) Horitani, M.; Offenbacher, A. R.; Marcus Carr, C. A.; Yu, T.; Hoeke, V.; Cutsail, G. E.; Hammes-Schiffer, S.; Klinman, J. P.; Hoffman, B. M. 13C ENDOR Spectroscopy of Lipoxygenase-Substrate Complexes Reveals the Structural Basis for C-H Activation by Tunneling. *J. Am. Chem. Soc.* 2017, *139* (5). https://doi.org/10.1021/jacs.6b11856.

(4) Skamnioti, P.; Gurr, S. J. Against the Grain: Safeguarding Rice from Rice Blast Disease. *Trends in Biotechnology*. 2009. https://doi.org/10.1016/j.tibtech.2008.12.002.

(5) Wennman, A.; Oliw, E. H.; Karkehabadi, S.; Chen, Y. Crystal Structure of Manganese Lipoxygenase of the Rice Blast Fungus Magnaporthe Oryzae. *J. Biol. Chem.* 2016, *291* (15). https://doi.org/10.1074/jbc.M115.707380.

(6) Nelson, M. J. Catecholate Complexes of Ferric Soybean Lipoxygenase 1. *Biochemistry* 1988, *27* (12). https://doi.org/10.1021/bi00412a011.

(7) Kostenko, A.; Ray, K.; Iavarone, A. T.; Offenbacher, A. R. Kinetic Characterization of the C-H Activation Step for the Lipoxygenase from the Pathogenic Fungus Magnaporthe

Oryzae: Impact of N-Linked Glycosylation. *Biochemistry* 2019, *58* (29). https://doi.org/10.1021/acs.biochem.9b00467.

(8) Su, C.; Sahlin, M.; Oliw, E. H. Kinetics of Manganese Lipoxygenase with a Catalytic Mononuclear Redox Center. *J. Biol. Chem.* 2000, *275* (25). https://doi.org/10.1074/jbc.M001408200.

(9) Su, C.; Oliw, E. H. Manganese Lipoxygenase. Purification and Characterization. *J. Biol. Chem.* 1998, *273* (21). https://doi.org/10.1074/jbc.273.21.13072.

(10) Newcomer, M. E.; Brash, A. R. The Structural Basis for Specificity in Lipoxygenase Catalysis. *Protein Science*. 2015. https://doi.org/10.1002/pro.2626.

(11) Hammarberg, T.; Provost, P.; Persson, B.; Rådmark, O. The N-Terminal Domain of 5-Lipoxygenase Binds Calcium and Mediates Calcium Stimulation of Enzyme Activity. *J. Biol. Chem.* 2000, *275* (49). https://doi.org/10.1074/jbc.M006136200.

(12) Kulkarni, S.; Das, S.; Funk, C. D.; Murray, D.; Cho, W. Molecular Basis of the Specific Subcellular Localization of the C2-like Domain of 5-Lipoxygenase. *J. Biol. Chem.* 2002, *277* (15). https://doi.org/10.1074/jbc.M112393200.

(13) Wecksler, A. T.; Kenyon, V.; Garcia, N. K.; Deschamps, J. D.; Van Der Donk, W. A.; Holman, T. R. Kinetic and Structural Investigations of the Allosteric Site in Human Epithelial 15-Lipoxygenase-2. *Biochemistry* 2009, *48* (36). https://doi.org/10.1021/bi9009242.

(14) Mogul, R.; Johansen, E.; Holman, T. R. Oleyl Sulfate Reveals Allosteric Inhibition of Soybean Lipoxygenase-1 and Human 15-Lipoxygenase. *Biochemistry* 2000, *39* (16).

https://doi.org/10.1021/bi992805t.

(15) Offenbacher, A. R.; Iavarone, A. T.; Klinman, J. P. Hydrogen-Deuterium Exchange Reveals Long-Range Dynamical Allostery in Soybean Lipoxygenase. *J. Biol. Chem.* 2018, *293* (4). https://doi.org/10.1074/jbc.M117.817197.

(16) Aoki-Kinoshita, K. F. Introduction to Glycobiology. In *Glycome Informatics: Methods and Applications*; 2019. https://doi.org/10.1201/9781420083361-1.

(17) Klinman, J. P.; Offenbacher, A. R. Understanding Biological Hydrogen Transfer Through the Lens of Temperature Dependent Kinetic Isotope Effects. *Acc. Chem. Res.* 2018, *51* (9). https://doi.org/10.1021/acs.accounts.8b00226.

(18) Klinman, J. P.; Offenbacher, A. R.; Hu, S. Origins of Enzyme Catalysis: Experimental Findings for C-H Activation, New Models, and Their Relevance to Prevailing Theoretical Constructs. *Journal of the American Chemical Society*. 2017. https://doi.org/10.1021/jacs.7b08418.

(19) Fenimore, P. W.; Frauenfelder, H.; McMahon, B. H.; Parak, F. G. Slaving: Solvent Fluctuations Dominate Protein Dynamics and Functions. *Proc. Natl. Acad. Sci. U. S. A.* 2002, *99* (25). https://doi.org/10.1073/pnas.212637899.

(20) Knapp, M. J.; Rickert, K.; Klinman, J. P. Temperature-Dependent Isotope Effects in Soybean Lipoxygenase-1: Correlating Hydrogen Tunneling with Protein Dynamics. *J. Am. Chem. Soc.* 2002, *124* (15). https://doi.org/10.1021/ja012205t.

(21) Offenbacher, A. R.; Sharma, A.; Doan, P. E.; Klinman, J. P.; Hoffman, B. M. The Soybean Lipoxygenase-Substrate Complex: Correlation between the Properties of Tunneling-Ready

States and ENDOR-Detected Structures of Ground States. *Biochemistry* 2020, *59* (7). https://doi.org/10.1021/acs.biochem.9b00861.

(22) Edwards, S. J.; Soudackov, A. V.; Hammes-Schiffer, S. Impact of Distal Mutation on Hydrogen Transfer Interface and Substrate Conformation in Soybean Lipoxygenase. *J. Phys. Chem. B* 2010, *114* (19). https://doi.org/10.1021/jp100133p.

(23) Soudackov, A. V.; Hammes-Schiffer, S. Proton-Coupled Electron Transfer Reactions: Analytical Rate Constants and Case Study of Kinetic Isotope Effects in Lipoxygenase. *Faraday Discuss.* 2016, *195*. https://doi.org/10.1039/c6fd00122j.

(24) Hatcher, E.; Soudackov, A. V.; Hammes-Schiffer, S. Proton-Coupled Electron Transfer in Soybean Lipoxygenase. *J. Am. Chem. Soc.* 2004, *126* (18). https://doi.org/10.1021/ja039606o.

(25) Soudackov, A. V.; Hammes-Schiffer, S. Probing Nonadiabaticity in the Proton-Coupled Electron Transfer Reaction Catalyzed by Soybean Lipoxygenase. *J. Phys. Chem. Lett.* 2014, *5* (18). https://doi.org/10.1021/jz501655v.

(26) Salna, B.; Benabbas, A.; Russo, D.; Champion, P. M. Tunneling Kinetics and Nonadiabatic Proton-Coupled Electron Transfer in Proteins: The Effect of Electric Fields and Anharmonic Donor-Acceptor Interactions. *J. Phys. Chem. B* 2017, *121* (28). https://doi.org/10.1021/acs.jpcb.7b05570.

(27) Hu, S.; Soudackov, A. V.; Hammes-Schiffer, S.; Klinman, J. P. Enhanced Rigidification within a Double Mutant of Soybean Lipoxygenase Provides Experimental Support for Vibronically Nonadiabatic Proton-Coupled Electron Transfer Models. *ACS Catal.* 2017, *7* (5). https://doi.org/10.1021/acscatal.7b00688.

(28) Cristea, M.; Engström, Å.; Su, C.; Hörnsten, L.; Oliw, E. H. Expression of Manganese Lipoxygenase in Pichia Pastoris and Site-Directed Mutagenesis of Putative Metal Ligands. *Arch. Biochem. Biophys.* 2005, *434* (1 SPEC. ISS.). https://doi.org/10.1016/j.abb.2004.10.026

II. Biophysical Characterization of the Impact of N-linked Glycosylation on Protein Structure and Proficiency of Enzymatic C-H Activation: Case Study of *Mo*LOX

Introduction

The large size and native flexibility of proteins is typically recognized as being critical for the formation of the enzyme-substrate complex and creation of protein allostery. This suggests a connection between the protein motions and the bond making-bond cleavage step of catalysis.[1] In the case of electron transfer reactions, the electron tunneling rate (Marcus) theory supports that the motions of heavy atoms play a critical role in facilitating wave function overlap for efficient transfer.[2] Similarly, hydrogen tunneling that describes the hydrogen transfer from enzymatic C-H activation focuses mainly on the internuclear distances between donor and acceptor and the role of the heavy atom motions, either from the substrate itself or in the protein as a whole, to provide transient active site compaction.[3,4] Lipoxygenases (LOXs) have emerged as a model system for enzymatic C-H activation that displays some of the largest primary deuterium kinetic isotope effects (KIE = k(H)/k(D); where H = protium and D = deuterium) around 100 at room temperature for both an enzymatic or solution C-H bond abstraction reaction.[5,6] After LOXs were determined to be a 'unique' model system for C-H activation reactions there arose a number of other enzymes with extremely large KIEs as well as an unusual fungal LOX that uses Mn(III)-OH as the active site oxidant.[7,8]

The temperature dependence of the kinetic isotope effect, ΔEa (ΔEa = Ea(D) – Ea(H)), has emerged as the most general and useful probe among these enzyme catalyzed C-H reactions.[9,10] The ΔEa value can be used as a link between the surface of the protein and its efficiency. ΔEa values of 0 are indicative of finely tuned tunneling in highly evolved enzymes while values that

increase from this are related to an impairment and often accompany change in the active site size or shape by site-directed mutagenesis.

A unique lipoxygenase from the rice blast fungus *Magnaporthe oryzae* (*Mo*LOX) has potentially emerged as a new model system for the relation between C-H activation and protein structure. It is considered a unique LOX for three main reasons: 1) it produces a unique bis-allylic hydroperoxide, 2) it has a manganese as its catalytic center instead of iron, and 3) it is decorated with multiple N-linked glycosylation on the protein surface. The bis-allylic product is unique and challenging to study due to the fact that there is no spectroscopic signature and must be tracked kinetically via consumption of the second substrate, molecular oxygen. The paramagnetic high spin (S=5/2) Mn^{2+} cofactor is useful in many biophysical techniques including electron paramagnetic resonance (EPR) and electron nuclear double resonance (ENDOR) spectroscopies. It is important to note that replacement of the Fe^{2+} center in the animal and plant LOXs with Mn^{2+} renders the enzyme inactive.[11] The replacement of manganese for iron in fungal LOXs has not been reported.

N-linked glycosylation modifications play an important role throughout nature; these post-translational modifications can influence the stability and solubility of a protein as well as serve as a cell signal mediator.[12] They are also clinically relevant since they are associated with congenital disorders, rheumatoid arthritis, and diabetes.[12,13] Specifically, *Mo*LOX contains N-linked glycans which are attached to an asparagine on the protein surface. The N-linked glycosylation that decorate the surface of the LOX have the potential to strongly influence the structure, stability, and folding of the protein itself, however, little is known about its role for *Mo*LOX structure and function.

In the literature, there is evidence of a link between changes at the protein surface, such as glycan removal or addition, and tuning of the active site itself.[14,15] Because of these glycans impede crystallization procedures, X-ray tools are often not applicable to the native glycoproteins. To address this question, HDX-MS has been used in this Chapter to reveal a dynamical link between the site of glycosylation and the active site and we show a dependence on the method for processing the N-linked glycosylation on *Mo*LOX. HDX-MS has previously been used to show a link between the desialylation of human erythropoietin (EPO) and the loosening of the overall structure.[14] From the study, they found that the majority of the exchange is around the 2 N-glycosylation and single O-glycosylation, with desialylation enhancing the dynamics in those regions.[14] It has also been shown that with degalactosylation of IgG1, there are conformational changes and increased D_2O uptake.[15] The study showed conversely that when IgG1 is hypergalactosylated the protein protects an important set of residues within the protein as well as increasing protein rigidity which in turn increases receptor binding.[15] These previous studies highlight the power of HDX-MS to study the protein structural impact of removing or altering the N-glycosylation sites.

In this chapter, the functional and structural impact of removing N-linked glycans from *Mo*LOX will be explored using kinetic isotope effects and HDX-MS. A series of 'deglycosylated' *Mo*LOX variants were prepared using Endo H, PNGase F, and asparagine to glutamine mutagenesis.

Methods

Materials

LA, γLA, αLA, and AA were purchased from Acros Organic, TCI (Palo Alto, CA), and Cayman Chemical Company (Ann Arbor, MI), respectively. Deuterium oxide (D_2O, 99% D), NaOD (99% D), and DCl (99% D) were purchased from Cambridge Isotopes (Tewksbury, MA). Dideuterated linoleic acid (11,11-D_2-LA) was synthesized previously.[16] All yeast/bacterial cells, media, salts, and buffers were purchased from Fisher Scientific, Sigma-Aldrich, or VWR at the highest grade possible.

MoLOX Expression and Purification

WT MoLOX was expressed in and purified from *P. pastoris* X-33 cells as previously described.[11,17] The 'Gln' mutant was generated from the mutagenesis of 8 asparagine residues forming predicted glycan sites (N18, N28, N48, N72, N150, N215, N501, and N535) to glutamine. This gene was generated by GenScript (Piscataway, NJ). Gln *Mo*LOX purification required the use of a butyl sepharose column for the initial capture via hydrophobic interaction chromatography (HIC). The final purification for all variants was carried out using a HiPrep 26/60 Sephacryl S-200 column on an AKTA FPLC system with 50 mM HEPES (pH 7.5), 150 mM NaCl, and 10% glycerol. The fractions that corresponded to the peak with lipoxygenase activity was concentrated to 100 μM, frozen in aliquots with N_2(l), and stored at -80 °C. Mn content was determined using ICP-MS.

Enzyme Kinetics

MoLOX enzyme kinetics were determined using a Hansatech oxygen (O_2) electrode. LA, dideuterated LA (11,11-D_2-LA), αLA, γLA, and AA concentrations were determined enzymatically. Kinetic parameters (k_{cat} and k_{cat}/K_M) were extracted from nonlinear fits to the Michaelis-Menten equation. Kinetic assays for pH dependence were performed at 20 °C in 0.1 M Tris-HCl (pH 7) or 0.1 M borate (pH 9) with substrate concentrations from 2-100μM. For temperature-dependent studies, kinetic assays were performed at 10, 12.5, 15, 20, 25, 27.5, and 30 °C and in 0.1 M borate (pH 9) with substrate concentrations ranging from 2 to 100 μM.

EndoH Deglycosylation

An endoglycosidase H (EndoH) from *Streptomyces plicatus* was optimized for recombinant expression in *E. coli* and subcloned in-line with his-tagged MBP construct (2CT-10 vector was a gift from Scott Gradia, Addgene plasmid #55209). Recombinant MBP-EndoH fusion was expressed in and purified from *E. coli* BL21 (DE3) cells. In brief, EndoH expression was induced by 1 mM IPTG once OD_{600} = 0.6. Upon induction, the cultures were dropped to 18 °C. Cells were lysed by sonication in lysis buffer (50 mM sodium phosphate, 100 mM NaCl, 8% glycerol, 2 mM $MgSO_4$, pH 7.5, supplemented with lysozyme, DNAse I, and AEBSF). The protein was purified using NiNTA chromatography, dialyzed in 50 mM Tris, 150 mM NaCl, pH 8 buffer and stored at -80°C until use.

EndoH *Mo*LOX was prepared by treating WT *Mo*LOX with EndoH in a 20:1 (*Mo*LOX:EndoH) mass ratio. The reaction was carried out at room temperature overnight in 50 mM sodium acetate, pH 5.5. The optimal reaction conditions were determined using SDS-PAGE. In our hands, the reaction did not require α-mannosidase for complete digestion. For large scale preparations, after the reaction, *Mo*LOX was

separated from MBP-EndoH by passing the reaction over a NiNTA column equilibrated with 50 mM Tris (pH 8), 500 mM NaCl and 10 mM imidazole and then further purification using SEC FPLC.

Circular Dichroism (CD)

Structure will be assessed by CD using a Jasco model J-815 CD spectrometer at room temperature with bandwidths of 2 nm with a Starna cell (path length of 0.1 cm). Samples were recorded at 25°C in 25 mM potassium phosphate (pH 7). The concentrations (typically 3 μM) were adjusted so that the PMT high voltage (HT) remained ≤ 600V in the range of 190-260 nm. Measurements for stability were also carried out with wavelengths set to 222 nm and the temperature range of 25-90°C (2°C intervals) with a temperature ramp up rate of 0.6°C/min.

Hydrogen-deuterium exchange- Mass spectrometry (HDX-MS)

Peptide from the pepsin digested WT MoLOX were previously assigned using LC-MS/MS.[11] Using these peptides, HDX measurements were carried out through 10-fold dilution of MoLOX (WT, EndoH, Gln) in 10 mM HEPES (pD 7.5), 150 mM NaCl D_2O buffer. Samples were incubated on a water bath at 20 °C. At a specified time, a sample was cold (-20 °C bath) and acid quenched (to pH 2.4) to minimize back-exchange. The samples were digested with immobilized pepsin for 2.5 minutes. Prior to digestion, guanidine HCl (pH 2.4) was added to a final concentration of 0.5 M. The pepsin was removed by filtration and the samples were flash frozen in liquid N_2 and stored at -80°C until data collection.

Deuterated, pepsin-digested samples of *Mo*LOX from HDX experiments were analyzed using an Agilent 1200 LC (Santa Clara, CA) that was connected in-line with the LTQ Orbitrap XL

mass spectrometer (Thermo). Data acquisition was controlled using Xcalibur software (version 2.0.7, Thermo). Mass spectral data acquired for HDX measurements were analyzed using the software, HDX WorkBench.[18] The percent deuterium incorporation for each peptide has been normalized for 100% D_2O and corrected for peptide-specific back-exchange, as previously described.[19]

Results and Discussion

Protein Expression and Purification

Wild-type (WT) *Mo*LOX was expressed as previously described[11] and purified via phenyl Sepharose column and size-exclusion FPLC. Typical yields of WT *Mo*LOX were around 10-12 mg/mL and these yields were then used to make the PNGase and EndoH variants of *Mo*LOX. The Gln *Mo*LOX variant showed slightly lower yields of around 5-6 mg/mL. SEC-FPLC and SDS-PAGE were used to corroborate the change in mass with deglycosylation. The SDS-PAGE showed an altered migration consistent with a decrease in mass that approaches the theoretical mass of the protein (67 kDa) (**Figure 2.1**). FPLC traces were used to show the solution mass of the EndoH variant (~70 kDa) was comparable to the theoretical mass of the enzyme, supporting a monomeric form of the protein. Thus, removal of N-linked glycosylation by EndoH doesn't lead to oligomerization. Secondary structure of the variants was confirmed to be intact and consistent with WT via CD traces (**Figure 2.1**). CD was also used to determine the thermostability of WT *Mo*LOX and its variants; this approach of altering the temperature of the CD provides the Tm of the enzyme. There was a noticeable difference in the Tm of the Gln variant with a Tm of 54.3 ± 0.3 °C compared

the wt with a Tm of 59.8±0.2 °C while PNGaseF and EndoH have a slight reduction in Tm, with a Tm of 57.8±0.3 °C and 55.5±0.3 °C, respectively (**Table 2.1**).

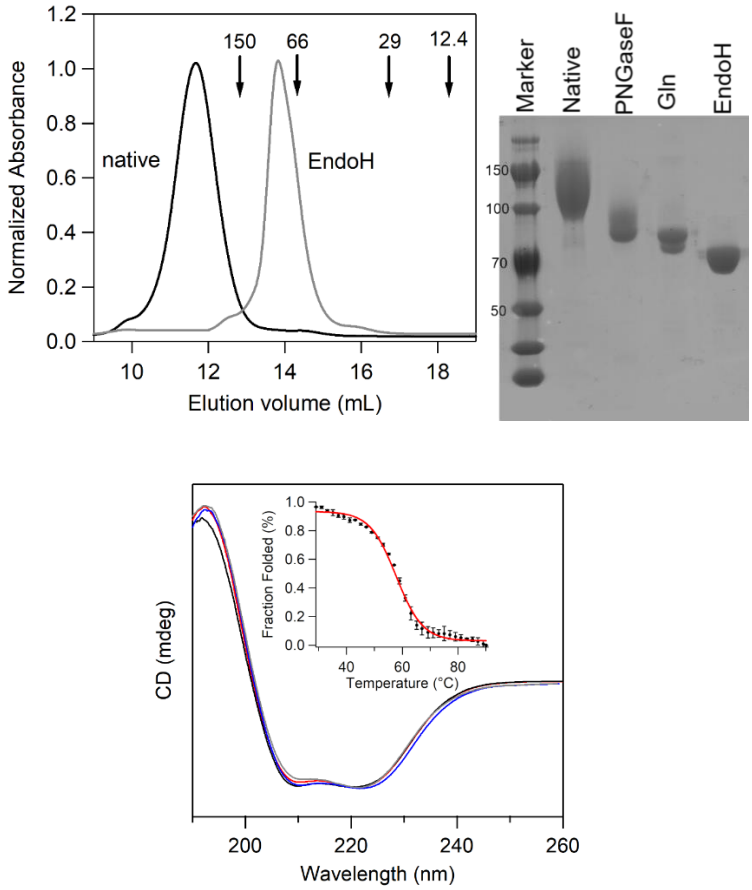

Figure 2.1: *FPLC traces, SDS-PAGE, and CD traces of native and deglycosylation MoLOX variants*

Table 2.1: *Thermostability of MoLOX variants*

MoLOX variant	**Tm (°C)**
Native (WT)	59.8 ± 0.2
EndoH	55.5 ± 0.3
PNGaseF	57.8 ± 0.3
Gln	54.3 ± 0.3
N72Q	62.2 ± 0.6
N215Q	58.2 ± 0.3

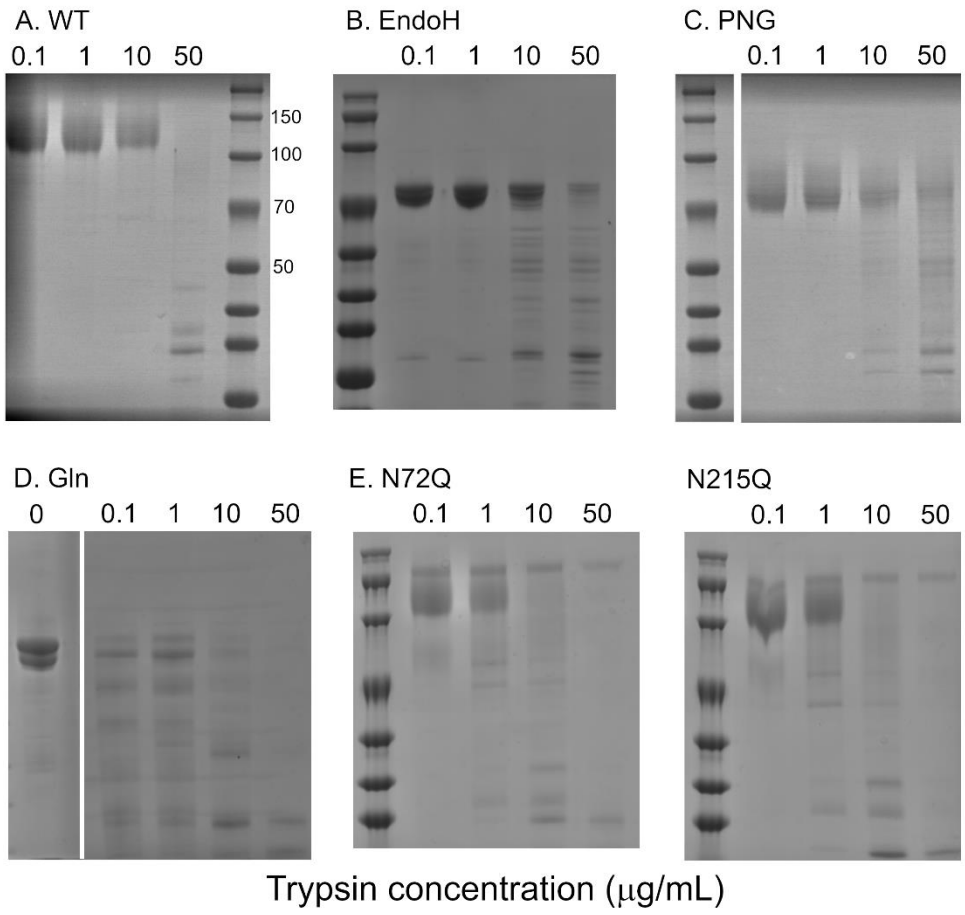

Figure 2.2: *Proteolytic stability; WT, EndoH, PNG, Gln; N72Q, N215Q*

Next, the proteolytic stability of the different *Mo*LOX variants was tested with a trypsin digest experiment. Wild-type MoLOX showed degradation at a trypsin concentration of 50 μg/mL and the EndoH and PNGase showed an increase in degradation at lower trypsin concentrations, notable at 10 ug/mL of trypsin (**Figure 2.2**). The most extreme case of degradation was with the Gln mutant which showed protein degradation almost at all concentrations of trypsin. The data support that the N-linked glycosylation provide proteolytic stability of the *Mo*LOX enzyme. This may be biologically relevant as the *Mo*LOX enzyme is excreted by the fungus into the rice plant

and proposed to initiate pathogenesis of the fungus; the glycans are therefore likely to protect *Mo*LOX from being degraded by the rice proteases.

These results are consistent with recent reports on the removal of N-linked glycosylation of the RNaseA enzyme.[20] This could be the reason behind the lower expression of Gln *Mo*LOX when compared to wt *Mo*LOX.

Catalytic Parameters

Previous work in the Offenbacher lab with the PNGaseF treated *Mo*LOX showed an increase in k_{cat} from 2.41 s^{-1} for wt to 3.0 s^{-1} for the treated *Mo*LOX (**Table 2.2**). This represents a slight increase in the catalytic activity of the enzyme with treatment and paired with a decrease in k_{cat}/K_M (0.13 μM^{-1} s^{-1} from 0.17 μM^{-1} s^{-1} in wt). The E_a of the PNG treated mutant is similar to the wt variant but the change in ΔE_a is large enough to raise the question if the substrate is sitting in the active site differently than wt but this requires more investigation to accurately determine.

EndoH treated *Mo*LOX shows a similar k_{cat} (2.38±0.15 s^{-1}) with a lowered k_{cat}/K_M (0.12±0.02 μM^{-1} s^{-1}) but interestingly shows a large increase in E_a from 9.6±0.5 kcal/mol to 15.2±1.0 kcal/mol when compared to wt. This shows a large change in the active site environment which is causing this increase but interestingly the ΔE_a is still similar to wt.

The Gln mutant shows a significant increase in k_{cat} (2.97±0.2 s^{-1}) which is similar to the PNG treated *Mo*LOX as well as a large increase in k_{cat}/K_M (0.34±0.08 μM^{-1} s^{-1} from 0.17±0.03 μM^{-1} s^{-1}). There is also a slight increase in E_a but the ΔE_a is similar to wt *Mo*LOX.

Table 2.2: *Kinetic parameters for MoLOX variants and their reactions with substrate LA*[a]

	k_{cat}[a] (s^{-1})	k_{cat}/K_M ($\mu M^{-1}s^{-1}$)	E_a(H) (kcal/mol)	$^{D}k_{cat}$[b]	ΔE_a (kcal/mol)
MoLOX	2.41±0.2	0.17±0.03	9.6±0.5	70±2	-1 ± 0.6
PNGaseF[c]	3.0±0.1	0.13±0.02	9.7±0.6	73±3	0.6 ± 0.6
EndoH	2.38±0.15	0.12±0.02	15.2±1.0	70±6	-0.9 ± 1.5
Gln	2.97±0.2	0.34±0.08	12.1±0.7	57±5	-1.1 ± 0.8

[a]Conditions: 0.1 M borate, pH 9.0; temp = 20 °C. [bD]k_{cat} = k_{cat}(H)/k_{cat}(D); temp = 20 °C. [c]Kinetic parameters from ref 11

Substrate Selectivity

Substrate selectivity of WT *Mo*LOX and the various mutants was determined by measuring the first- (k_{cat}) and second-order rate constants (k_{cat}/K_M) of different substrates and compared these values to linoleic acid (LA). Note that LA is the predominant unsaturated fatty acid in rice.[21] The other substrates chosen were alpha and gamma linolenic acid (α- and γLA) as well as the non-physiologically-relevant substrate, arachidonic acid (AA). When the *Mo*LOX variants were examined for k_{cat} all the *Mo*LOX variants showed the same speed of reaction for all the substrates (**Table 2.3 and Figure 2.3A**). In all cases, the order of the rate of substrate oxidation was (from fastest to slowest): αLA > LA > AA > γLA. The rates of αLA and LA were the same as reported for the WT *Mo*LOX previously.[22]

When determining k_{cat}/K_M, WT the PNGase and EndoH *Mo*LOX variants showed an increase in substrate preference for αLA and AA (not available in plants) over the LA substrate (**Table 2.3 and Figure 2.3B**). Conversely the Gln mutant showed an increase towards LA for all substrates when compared to LA. Most of the variants (excluding PNGase) had a lower preference for γLA when compared to LA. The difference in the Gln form compared to WT and other MoLOX variants accompanies the observed overall increase in k_{cat}/K_M for LA, supporting a link

between the presence of the surface N-linked glycans and the active site as determined by an increased catalytic proficiency for LA.

Table 2.3: *Substrate selectivity ratios of first- and second-order rate constants for MoLOX variants at 20 °C and pH 9.*

	k_{cat} (s^{-1})			k_{cat}/K_M ($\mu M^{-1}s^{-1}$)		
	αLA/AA	**γLA/LA**	**AA/LA**	**αLA/LA**	**γLA/LA**	**AA/LA**
WT	1.81±0.19	0.26±0.02	0.48±0.03	1.79±0.66	0.79±0.23	1.59±0.51
EndoH	1.85±0.16	0.29±0.02	0.42±0.03	1.98±0.61	0.91±0.36	2.72±0.72
Gln	1.69±0.14	0.22±0.01	0.42±0.03	0.61±0.18	0.38±0.12	0.72±0.24
PNG	1.62±0.25	0.22±0.03	0.32±0.04	2.31±1.0	1.09±0.58	1.02±0.47

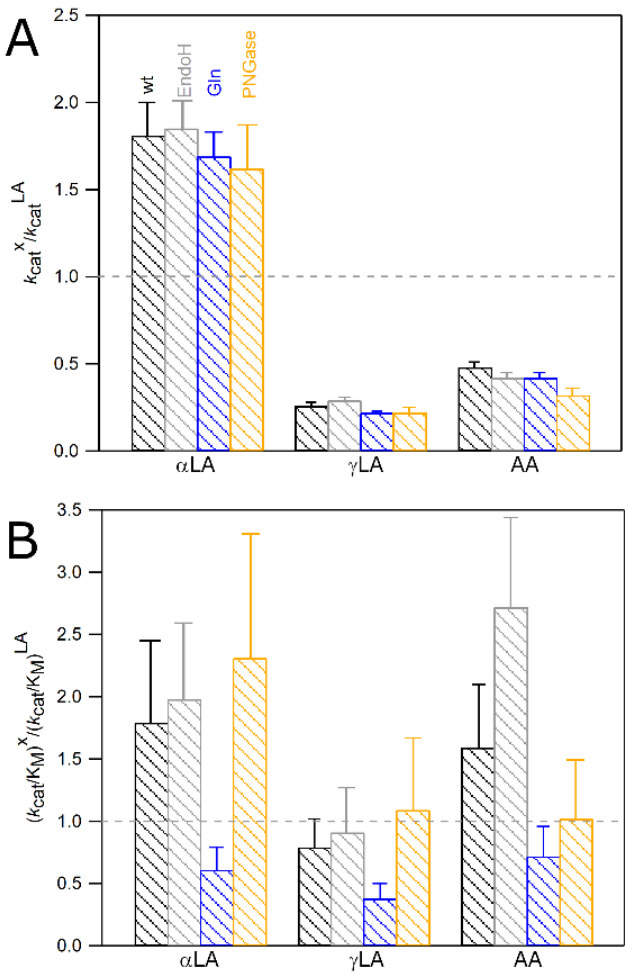

Figure 2.3: *Substrate selectivity ratios for WT (black), EndoH (gray), Gln (blue), and PNGase (orange) MoLOX variants. Kinetics were collected non-competitively at 20°C in 0.1 M borate, pH 9.0 buffer. See Table 2.3 for list of values.*

HDX-MS of wild-type MoLOX

To provide structural insight into the dynamical link between the site of N-linked glycans and the active site, hydrogen-deuterium exchange (HDX) experiments were performed. HDX allows us to look at protein flexibility in a regionally defined manner when coupled to proteolytic digestion by pepsin and analysis of regional deuterium uptake by mass spectrometry (MS). This

exchange is particularly informative when comparing the wild-type protein to different mutants with altered function to determine the impacts on protein structure and dynamics.

From the 274 total peptides assigned from tandem MS experiments of pepsin-digested WT *Mo*LOX, we have identified 33 non-overlapping peptides that correspond to a coverage of 79%. Non-overlapping peptides were used for data reduction purposes. Note that the first 55 residues were not resolved in the coverage. The poor coverage in this region is likely due to the high glycosylation (N18, N28, and N48) content at the N-terminus that could prevent access for pepsin to process this area.

Figure 2.4 presents the HDX-MS behavior (in percent exchange) at 2 hours and 20 °C mapped onto the structural model of *Mo*LOX determined from X-ray (PDB: 5FNO). Overall, the exchange pattern is expected based on the LOX fold (**Figure 2.4**) and is fairly consistent with the X-ray derived B-factors (**Figure 2.4B**). For example, there is a high amount of exchange at the helix α2 and for part of helix 11 – also referred to as the 'arched helix', which lines the entrance to the active site of the enzyme. Conversely, the core of the protein exhibited very low (<20 %) exchange.

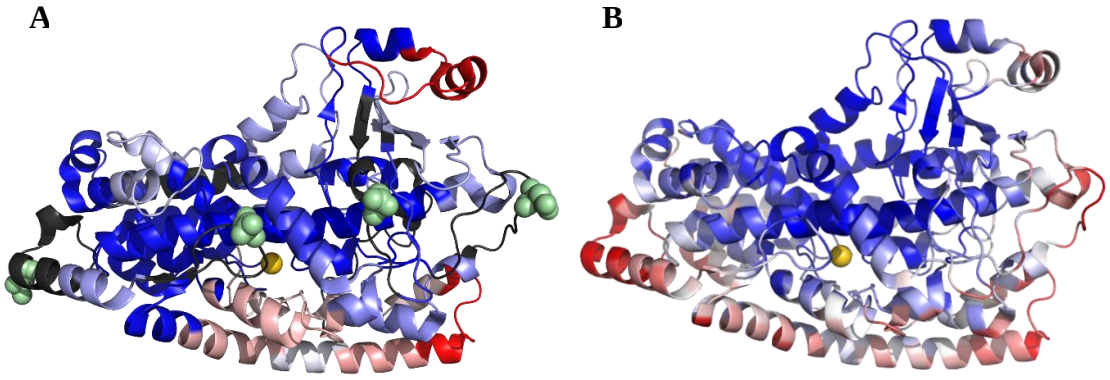

Figure 2.4: *HDX-MS behavior of MoLOX at 20 °C and 2 h (A) compared to the X-ray derived B-factors (B). The color corresponds to: blue (0-30% HDX), white (31-60% HDX), and red (>60% HDX).*

When comparing the HDX behavior of *Mo*LOX to two other canonical LOXs, soybean (SLO) from plants[23] and 15-LOX-2 from human, (unpublished results from Offenbacher Lab) overall, the exchange is comparable with only two notable exceptions (**Figure 2.5 A-C**). With SLO and 15-LOX-2 there is a greater extent of exchange at helix α2. In these enzymes, the helical structure is bent or broken at the N-terminal portion, but in *Mo*LOX, the α2 helix nearly traverses the entire length of the catalytic domain. This exchange pattern is functionally significant because the α2 helix is considered to play an important role in regulating substrate binding and activity.[8] From our lab's previous kinetic analysis of *Mo*LOX, we have found that *Mo*LOX substrate binding is *not* regulated by allostery which contrasts the SLO and human 15LOX2 isozymes. This lack of allosteric regulation was determined by the isotope effect on the second-order rate constant, $^{D}k_{cat}/K_M$, as a function of temperature and pH for the LA substrate. In the case of the well-characterized SLO, at elevated (>25 °C) temperatures, the $^{D}k_{cat}/K_M$ (*ca.* 40) approaches the large magnitude of the kinetic isotope effect on the first-order rate constant, $^{D}k_{cat}$ = 80. As the temperature is lowered to 5 °C, the value of the $^{D}k_{cat}/K_M$ for the SLO reaction with LA drastically drops to *ca.* 7-10, so that $^{D}k_{cat}/K_M << {}^{D}k_{cat}$. Under this case, substrate binding becomes (partially) rate-determining. However, addition of an allosteric effector to SLO under these conditions causes an elevation of the $^{D}k_{cat}/K_M$ to equal $^{D}k_{cat}$. Conversely, in the case of *Mo*LOX, the $^{D}k_{cat}/K_M$ value is nearly identical to the $^{D}k_{cat}$ from 10-30 °C and pH 7-9. These kinetic data support that the C-H bond cleavage step is fully rate determining for *Mo*LOX. The combination of the well-structured helix for α2 and the reduced HDX-MS behavior of this helical peptide further supports the kinetic results and implicates that it will likely not play a role in substrate selectivity/acquisition.

In addition to an altered HDX behavior for helix α2, compared to model plant and animal LOXs, *Mo*LOX showed a higher exchange extent at helix 11 (**Figure 2.5 B&C**) that includes the

conserved leucine (L331 in *Mo*LOX). Note that this increased exchange at helix 11 arises with decreased exchange to helix α2. Based on this unique exchange behavior, we propose that helix-11 likely plays an important role in controlling active site reactivity and potentially substrate selectivity.

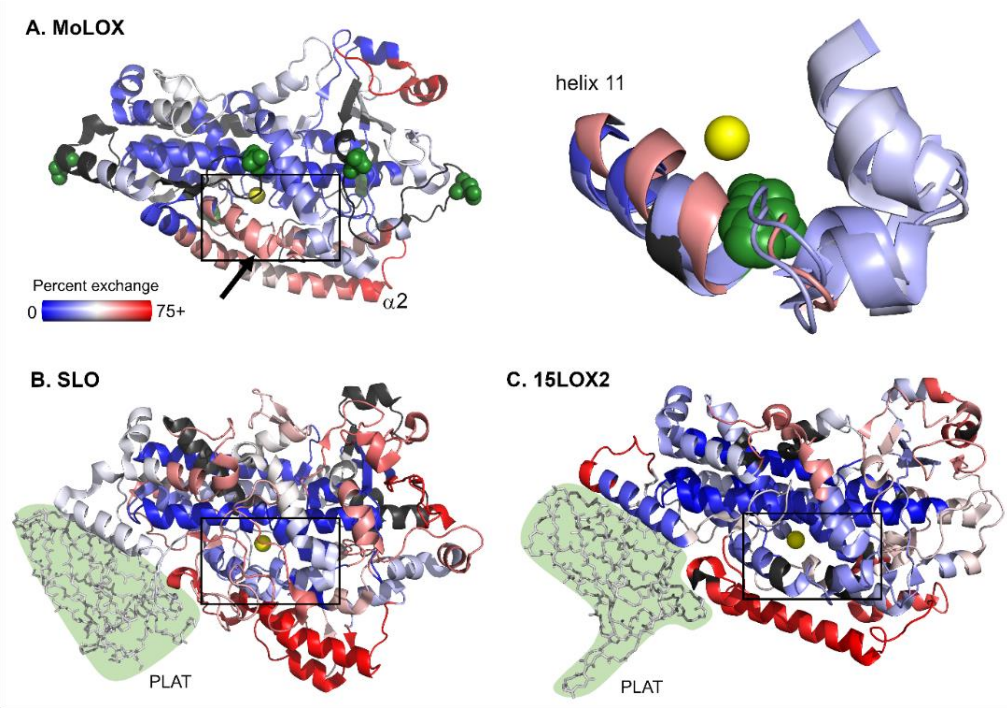

Figure 2.5: *Map of HDX-MS for WT MoLOX collected at 20°C (A). The catalytic metal is represented as a yellow sphere and the Asn residues that form glycosidic bonds are shown as green spheres. The black arrow represents the putative substrate entrance portal. (B) and (C) show the comparative HDX-MS maps previously reported for the paradigmatic plant (SLO[23]) and animal (15LOX2(unpublished results from Offenbacher Lab)) lipoxygenases, respectively. The N-terminal 'PLAT' (green shading) is a regulatory domain, not present in fungal LOXs. The alpha helix 11 (highlighted by box) in A-C are overlaid in the top right. The conserved leucine residue (L331, MoLOX; L546, SLO; L420, 15LOX2) is shown for reference.*

HDX of MoLOX Variants

To provide a basis for the structural and dynamical impact of removing N-linked glycosylation on *Mo*LOX, HDX-MS experiments were further performed on the EndoH, and Gln variants of *Mo*LOX. HDX-MS data were analyzed for EndoH and Gln variants in a similar manner to WT *Mo*LOX. Comparison of the 33 non-overlapping peptides identified six peptides that exhibit differences between WT and the Gln and/or EndoH variants of *Mo*LOX were restricted to two regions and are presented in Figure 2.6. Among these differences included active site residues 329-363 (helix 11), in which the Gln mutant showed an overall increase in percent exchange which corresponds to an increase in local protein flexibility. These peptides are flanked by two N-linked glycosylation sites, N72 and N215. In this region there are some instances of EndoH increasing the percent exchange but at helix 11 (329-337), EndoH treatment is linked to a decrease in exchange. This is an important set of residues since it coincides with helix 11 which controls the ability of the substrate to enter the active site. A second region of protein was also impacted, including residues 114-134 (C-terminal end of α2 helix) and 253-267. The same trends are also shown in these regions with EndoH causing a reduced percentage of exchange and the Gln mutant causing a slightly increased percent of exchange.

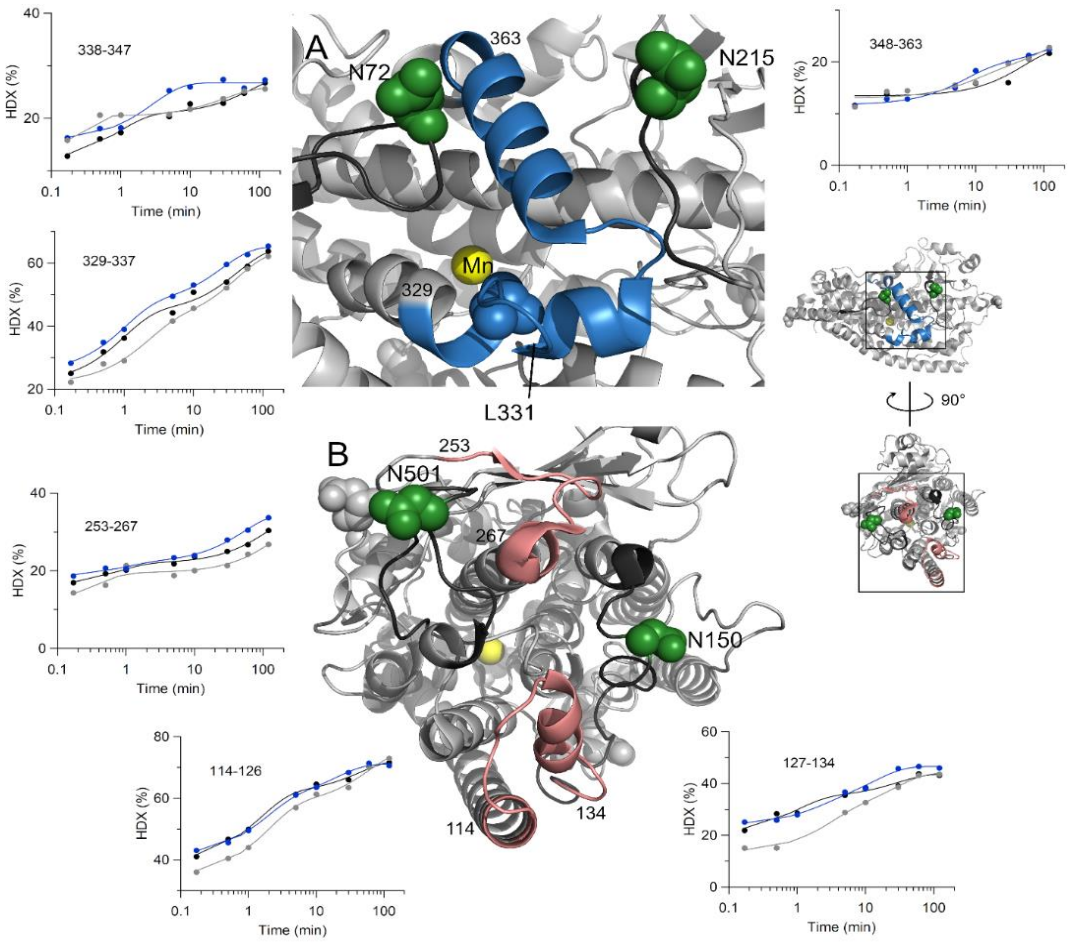

Figure 2.6: *HDX-MS traces, collected at 20°C, highlighting the differences between WT (black), EndoH (gray), Gln (blue) MoLOX.*

Single N-linked Glycan Knock-out MoLOX Variants

With the results emerging from the HDX-MS analysis, it was predicted that the dramatic effects of deglycosylation on active site proficiency likely originated from the one select N-linked glycan sites adjacent to the active site, including N72 and N215. Residues 72 and 215 were each singly converted from Asn to Gln. These two protein variants were expressed and isolated from yeast cultures similar to WT *Mo*LOX. These single knock-out mutants both have a Tm that is consistent with wt MoLOX, but have a proteolytic digest profile between EndoH and Gln variants

with degradation beginning slightly at 1 μg/mL and complete degradation at 10 and 50 μg/mL (**Table 2.1 and Figure 2.2**). Steady-state kinetic studies were performed (k_{cat} and k_{cat}/K_M), and substrate selectivity was tested using the various substrates and compared to LA. As shown in Table 2.4, the N72Q single mutant showed a significant increase in the second-order rate constant for LA ($0.34 \pm 0.07\ \mu M^{-1}s^{-1}$) compared to WT ($0.17 \pm 0.03\ \mu M^{-1}s^{-1}$) and matches the level of the fully Gln variant ($0.34 \pm 0.08\ \mu M^{-1}s^{-1}$). The N215Q single mutation, conversely, showed only a slight increase in the second-order rate constant that is nearly within error to the WT protein. Steady-state analysis was extended to the panel of substrates to assess selectivity (**Table 2.4**). Overall, the comparative second-order rate constants of N72Q were seen to track the Gln mutant for αLA/LA and γLA/LA while the N215Q reactivity more closely resembled the WT *Mo*LOX for αLA/LA. Both enzyme mutants exhibited AA/LA substrate selectivity ratios different than Gln or WT, suggesting that the molecular basis that controls substrate capture as a function of glycosylation state is complex and may not controlled by a single glycosylation site.

Table 2.4: *Substrate selectivity ratios for WT and N→Q MoLOX variants at pH 9 and 20°C.*

	k_{cat} LA (s^{-1})	**k_{cat}/K_M, LA ($\mu M^{-1}s^{-1}$)**	**k_{cat}/K_M ($\mu M^{-1}s^{-1}$)**		
			αLA/LA	**γLA/LA**	**AA/LA**
WT	2.41±0.2	0.17±0.03	1.79±0.66	0.79±0.23	1.59±0.51
Gln	2.97±0.2	0.34±0.08	0.61±0.18	0.38±0.12	0.72±0.24
N72Q	2.64±0.1	0.34±0.07	0.87±0.29	0.22±0.07	0.48±0.13
N215Q	2.52±0.1	0.24±0.06	1.55±0.52	0.46±0.14	0.52±0.16

References

(1) Klinman, J. P. Importance of Protein Dynamics during Enzymatic C-H Bond Cleavage Catalysis. *Biochemistry* **2013**, *52* (12). https://doi.org/10.1021/bi301504m.

(2) Marcus, R. A. On the Theory of Oxidation-Reduction Reactions Involving Electron Transfer. I. *J. Chem. Phys.* **1956**, *24* (5). https://doi.org/10.1063/1.1742723.

(3) Kuznetsov, A. M.; Ulstrup, J. Proton and Hydrogen Atom Tunnelling in Hydrolytic and Redox Enzyme Catalysis. *Can. J. Chem.* **1999**, *77* (5–6). https://doi.org/10.1139/cjc-77-5-6-1085.

(4) Knapp, M. J.; Klinman, J. P. Environmentally Coupled Hydrogen Tunneling: Linking Catalysis to Dynamics. *European Journal of Biochemistry*. 2002. https://doi.org/10.1046/j.1432-1033.2002.03022.x.

(5) Glickman, M. H.; Wiseman, J. S.; Klinman, J. P. Extremely Large Isotope Effects in the Soybean Lipoxygenase-Linoleic Acid Reaction. *J. Am. Chem. Soc.* **1994**, *116* (2). https://doi.org/10.1021/ja00081a060.

(6) Roecker, L.; Meyer, T. J. Hydride Transfer in the Oxidation of Alcohols by [(Bpy)2(Py)Ru(O)]2+. A KH/KDKinetic Isotope Effect of 50. *J. Am. Chem. Soc.* **1987**, *109* (3). https://doi.org/10.1021/ja00237a019.

(7) Hamberg, M.; Su, C.; Oliw, E. Manganese Lipoxygenase. Discovery of a Bis-Allylic Hydroperoxide as Product and Intermediate in a Lipoxygenase Reaction. *J. Biol. Chem.* **1998**, *273* (21). https://doi.org/10.1074/jbc.273.21.13080.

(8) Hoffmann, I.; Hamberg, M.; Lindh, R.; Oliw, E. H. Novel Insights into Cyclooxygenases, Linoleate Diol Synthases, and Lipoxygenases from Deuterium Kinetic Isotope Effects and Oxidation of Substrate Analogs. *Biochim. Biophys. Acta - Mol. Cell Biol. Lipids* **2012**, *1821* (12). https://doi.org/10.1016/j.bbalip.2012.09.001.

(9) Klinman, J. P.; Kohen, A. Hydrogen Tunneling Links Protein Dynamics to Enzyme Catalysis. *Annual Review of Biochemistry*. 2013. https://doi.org/10.1146/annurev-biochem-051710-133623.

(10) Klinman, J. P. A New Model for the Origin of Kinetic Hydrogen Isotope Effects. *J. Phys. Org. Chem.* **2010**, *23* (7). https://doi.org/10.1002/poc.1661.

(11) Kostenko, A.; Ray, K.; Iavarone, A. T.; Offenbacher, A. R. Kinetic Characterization of the C-H Activation Step for the Lipoxygenase from the Pathogenic Fungus Magnaporthe Oryzae: Impact of N-Linked Glycosylation. *Biochemistry* **2019**, *58* (29). https://doi.org/10.1021/acs.biochem.9b00467.

(12) Aoki-Kinoshita, K. F. Introduction to Glycobiology. In *Glycome Informatics: Methods and Applications*; 2019. https://doi.org/10.1201/9781420083361-1.

(13) Bermingham, M. L.; Colombo, M.; McGurnaghan, S. J.; Blackbourn, L. A. K.; Vučković, F.; Baković, M. P.; Trbojević-Akmačić, I.; Lauc, G.; Agakov, F.; Agakova, A. S.; Hayward, C.; Klarić, L.; Palmer, C. N. A.; Petrie, J. R.; Chalmers, J.; Collier, A.; Green, F.; Lindsay, R. S.; Macrury, S.; McKnight, J. A.; Patrick, A. W.; Thekkepat, S.; Gornik, O.; McKeigue, P. M.; Colhoun, H. M. N-Glycan Profile and Kidney Disease in Type 1 Diabetes. *Diabetes Care* **2018**, *41* (1). https://doi.org/10.2337/dc17-1042.

(14) Wang, A. L.; Zhou, Y.; Palmieri, M. J.; Hao, G. G. Hydrogen Deuterium Exchange

Reveals Changes to Protein Dynamics of Recombinant Human Erythropoietin upon N- and O- Desialylation. *J. Pharm. Biomed. Anal.* **2018**, *154*. https://doi.org/10.1016/j.jpba.2018.02.060.

(15) Houde, D.; Peng, Y.; Berkowitz, S. A.; Engen, J. R. Post-Translational Modifications Differentially Affect IgG1 Conformation and Receptor Binding. *Mol. Cell. Proteomics* **2010**, *9* (8). https://doi.org/10.1074/mcp.M900540-MCP200.

(16) Offenbacher, A. R.; Zhu, H.; Klinman, J. P. Synthesis of Site-Specifically13C Labeled Linoleic Acids. *Tetrahedron Lett.* **2016**, *57* (41). https://doi.org/10.1016/j.tetlet.2016.08.071.

(17) Wennman, A.; Jernerén, F.; Magnuson, A.; Oliw, E. H. Expression and Characterization of Manganese Lipoxygenase of the Rice Blast Fungus Reveals Prominent Sequential Lipoxygenation of α-Linolenic Acid. *Arch. Biochem. Biophys.* **2015**, *583*. https://doi.org/10.1016/j.abb.2015.07.014.

(18) Pascal, B.; Willis, S.; Lauer, J.; Landgraf, R.; West, G.; Marciano, D.; Novick, S.; Goswami, D.; Chalmers, M.; Griffin, P. HDX Workbench: Software for the Analysis of H/D Exchange MS Data. *J. Am. Soc. Mass Spectrom.* **2012**, *23* (9). https://doi.org/10.1021/jasms.8b04350.

(19) Hoofnagle, A. N.; Resing, K. A.; Ahn, N. G. Protein Analysis by Hydrogen Exchange Mass Spectrometry. *Annual Review of Biophysics and Biomolecular Structure*. 2003. https://doi.org/10.1146/annurev.biophys.32.110601.142417.

(20) Ressler, V. T.; Raines, R. T. Consequences of the Endogenous N-Glycosylation of Human Ribonuclease 1. *Biochemistry* **2019**, *58* (7). https://doi.org/10.1021/acs.biochem.8b01246.

(21) Brash, A. R. Lipoxygenases: Occurrence, Functions, Catalysis, and Acquisition of Substrate. *Journal of Biological Chemistry*. 1999. https://doi.org/10.1074/jbc.274.34.23679.

(22) Cristea, M.; Engström, Å.; Su, C.; Hörnsten, L.; Oliw, E. H. Expression of Manganese Lipoxygenase in Pichia Pastoris and Site-Directed Mutagenesis of Putative Metal Ligands. *Arch. Biochem. Biophys.* **2005**, *434* (1 SPEC. ISS.). https://doi.org/10.1016/j.abb.2004.10.026.

(23) Offenbacher, A. R.; Hu, S.; Poss, E. M.; Carr, C. A. M.; Scouras, A. D.; Prigozhin, D. M.; Iavarone, A. T.; Palla, A.; Alber, T.; Fraser, J. S.; Klinman, J. P. Hydrogen-Deuterium Exchange of Lipoxygenase Uncovers a Relationship between Distal, Solvent Exposed Protein Motions and the Thermal Activation Barrier for Catalytic Proton-Coupled Electron Tunneling. *ACS Cent. Sci.* **2017**, *3* (6). https://doi.org/10.1021/acscentsci.7b00142.

Appendix A

Reproduced with permission from ACS Books
Book: "Bridging Structure and Function in Mechanistic Enzymology"
Manuscript ID: bk-2020-0089k.R2
Title: "Tunneling Through the Barriers: Resolving the Origins of the Activation of C-H Bonds Catalyzed by Enzymes"
Authors: Chris Whittington, John Latham, and Adam R. Offenbacher

Enzymes have extraordinary catalytic power. This property has spawned decades of research to derive a full understanding into the origins of enzyme catalysis. Herein, the generalized mechanism of C-H activation (C-H bond cleavage), a prevalent enzyme reaction type that is often overlooked in biochemical textbooks, will be introduced. Years of experimental and computational evidence support that enzyme catalyzed C-H bond cleavage occurs through a non-classical (tunneling) mechanism. The ability of stable isotope labeling enables the examination of bond selective kinetic isotope effects, yielding a unique view into the entire shape of the kinetic barriers of catalysis. Results stemming from these enzymes, including the paradigm system, soybean lipoxygenase, have provided new insight into how enzymes 'work'. These catalytic principles will be highlighted with particular emphasis on the interpretation of the temperature dependence of the reaction rates for enzymatic C-H activation

Introduction to Enzyme Catalysis

Enzymes are remarkable catalysts that carry out an immense and diverse repertoire of chemical transformations that are essential to sustain life. As with any catalyst, an enzyme is defined by its ability to reduce the energetic barrier of a chemical reaction and, in turn, to accelerate the reaction rate (k_{obs}) compared to the noncatalyzed rate (k_{non}). Just how impressive are enzyme rate enhancements? While many enzyme systems are associated with k_{obs} values in the 10^0 to 10^4 s^{-1} range (**Table A.1**), the equivalent uncatalyzed reactions (at room temperature) may require hours, days, decades, or longer.[1]

There are a few extreme cases of rate enhancements by natural enzymes.[2] One example is the well-studied orotidine 5'-phosphate (OMP) decarboxylase which catalyzes the essential last step in the formation of pyrimidines in nucleic acid synthesis (**Scheme A.1A**).[3] Wolfenden provided evidence in the 1990's suggesting that the half-life for the nonenzymatic reaction (i.e. absence of enzyme) of forming pyrimidines is approximately 78 million (7.8×10^7) years at room temperature. As humans only have a lifespan of at most 100 years, assessment of the latter requires a bit of ingenuity to determine accurately and reasonably in a laboratory setting. To achieve the nonenzymatic reaction rate half-life, Wolfenden's team employed the strategy of heating the reaction vessels to 100°C (and above in sealed quartz cells), as solution reactions accelerate with increasing temperature. In the case of the nonenzymatic OMP decarboxylation, the reaction using the model reactant, 1-methyloroctic acid, was monitored at various temperature up to 200°C with a half-life of 19 hours while the half-life at 140°C was approximately 3-orders of magnitude slower.[2] The reported room temperature half-life of 78 million years was estimated from the Arrhenius relationship. Compared to the first order rate constant for the enzymatic reaction, k_{cat},

of 39 s^{-1}, the rate enhancement (k_{cat}/k_{non}) that OMP decarboxylase achieves is 1.4×10^{17} (**Table A.1**).

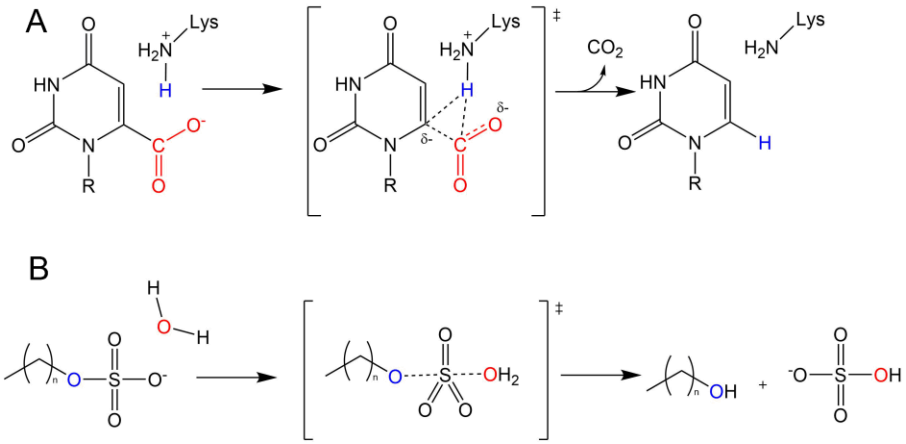

Scheme A.1. *Reaction schemes for (A) OMP decarboxylase and (B) S-O cleaving sulfatase.*

In 2012, an extreme case of enzymatic rate enhancement was reported for the S-O cleaving alkylsulfatases (**Scheme A.1B**). From this study, a k_{cat} of ~7 s^{-1} was observed compared to an estimated first-order rate constant for the noncatalytic reaction of $2x10^{-26}$ s^{-1} (half-life of 10^{18} years) yielding the gold-standard for enzymatic rate enhancement of 2 x 10^{26}-fold.[4]

Table A.1. *Rate enhancements of natural enzymes.*[2]

Enzyme	k_{cat} (s^{-1})	k_{obs}/k_{non}
S-O sulfatase	7	10^{26}
Phosphohydrolases	20-40	10^{21}
orotidine 5'-phosphate (OMP) decarboxylase	39	10^{17}
Staphylococcal nuclease	95	10^{14}
Carboxypeptidase	578	10^{13}
Cytidine deaminase	299	10^{12}
Ketosteroid isomerase	66,000	10^{11}
Carbonic anhydrase	10^6	10^6

How are enzymes capable of achieving such tremendous catalytic prowess? In 1948, Linus Pauling published a paper in the journal, *Nature*, that provided a persuasive suggestion of how enzymes work:[5]

> "I think that enzymes are molecules that are complementary in structure to the activated complexes of the reactions that they catalyze, that is, to the molecular configuration that is intermediate between the reacting substances and products of reaction for the catalyzed processes. The attraction of the enzyme molecule for the activated complex would thus lead to a decrease in its energy and hence to a decrease in energy of activation of the reaction and to an increase in the rate of reaction"

The term 'activated complex' is now understood as the transition state. The transition state is marked by the energy maximum along the reaction coordinate and is considered to resemble the reactive intermediate. Simply put, the 'Pauling principle' posits that enzyme rate acceleration is achieved by lowering the activation energy of the reaction through stabilization of the transition state. While it serves well as a definition of catalysis, it does not provide us with the physical origins for *how* enzymes greatly lower the energetic barrier(s) for catalysis.

Scientists have attempted to develop strategies to replicate nature's achievements, with the ultimate goal of designing an artificial catalyst (protein or otherwise) to carry out any desired reaction using 'green' conditions (room temperature, ambient pressure and non-toxic solutions). The strategies included the development of catalytic antibodies[6,7] as well as *de novo* enzymes[8]

developed by 'inside-out' computational design.[9,10] While select successful examples ensued, the catalytic power of these man-made catalysts have fallen short of natural enzymes with the upper limit rate enhancements of $\leq 10^9$ (See references[11–13], for select examples).

Since Pauling's publication nearly seventy years ago, there have been numerous advancements in our understanding of how enzymes achieve enormous rate accelerations. A few of the emerging principles, some framed by Pauling's model of transition state stabilization include, but not limited to, covalent catalysis[14–16], electrostatic catalysis[17,18], ground-state destabilization/desolvation effects[19,20], and proximity/orientation catalysis as well as other entropy reducing mechanisms.[21–23] Despite these advances, the Pauling principle is still commonly presented as the basis for enzyme catalysis in contemporary undergraduate biochemistry textbooks.

The above catalytic strategies focus greatly on the active site. However, enzymes are considerably large relative to their active sites and small molecule catalysts, with an average size of *ca.* 40 kDa (median human protein size is 375 amino acids with the average amino acid mass of 110 Da).[24] This raises the question into whether there exists synergy between the protein matrix and the achievement of active site proficiency. While the dynamic view of proteins is prominent for the binding of substrates and the release of products,[25,26] the discovery of quantum effects in enzyme catalyzed reactions, as seen for C-H bond cleavage (a.k.a. C-H activation), began to demonstrate the importance of protein motions *during* the chemical bond breaking/making steps of catalysis.[27–29] The central focus of this Chapter will be to introduce the reader to enzymatic C-H activation reactions in which extensive experimental and computational data provide compelling support for non-classical (i.e. quantum) behavior that in turn requires a break down of semi-

classical models of transition state theory (TST)[30,31] and emphasizes a role for conformational (thermal) motions that promotes transient active site precision.

C-H Activation Reactions in Biology

C-H activation (or C-H functionalization) is one of the most pervasive and fundamental reactions in both industrial and biologically catalyzed reactions. The process entails the cleavage of a sp^3-hybridized C-H bond (**Figure A.1**) and replacement with a C-X bond, where X is oxygen, nitrogen, or carbon. In organometallic chemistry, C-H activation is characterized as the cleavage of an unreactive C-H bond of alkanes, arenes, or alkyl chains using (rare, toxic and expensive) transition metal catalysts, forming a M-C bond, that can lead to its subsequent functionalization.[32]

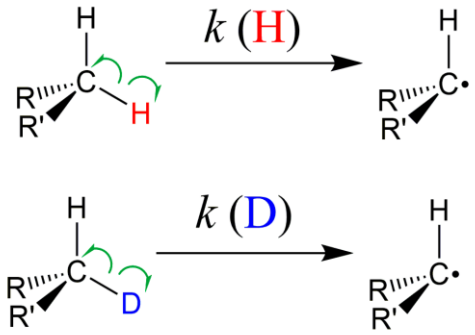

Figure A.1: *Diagram of homolytic C-H/C-D activation, resulting in the formal transfer of a hydrogen atom (H•). The C-H/C-D bond can also be cleaved through heterolytic processes, resulting in proton (H^+) and/or hydride (H^-) transfer.*

Enzyme-catalyzed C-H activation, prevalent in biological chemical transformations, is often mediated by a redox-active metallocofactor, such as iron, an organic centered radical formed through the transient oxidation of natural amino acids (e.g. tyrosine or cysteine), or a 5'-deoxyadenosyl radical derived from the homolytic cleavage of *S*-adenosyl methionine (SAM).[33,34] In contrast to the organic chemists' definition of C-H activation, these enzymatic reactions have

no evidence for formation of a direct metal-carbon bond. Instead, enzymes abstract a hydrogen atom to form a bound, transient substrate-centered radical that goes onto react intermolecularly or intramolecularly with oxygen, nitrogen, sulfur, or carbon to form the desired chemical transformation (**Figure A.2**). The diversity of enzymatic reactions that undergo radical C-H activation is considerable and include difficult reactions such as peroxidation,[35] hydroxylation,[36] methylation,[37] epimerization,[38] decarboxylation,[39] C-C bond formation,[40,41] C-S bond formation,[42,43] and other C-O bond formations[44] to name a few.

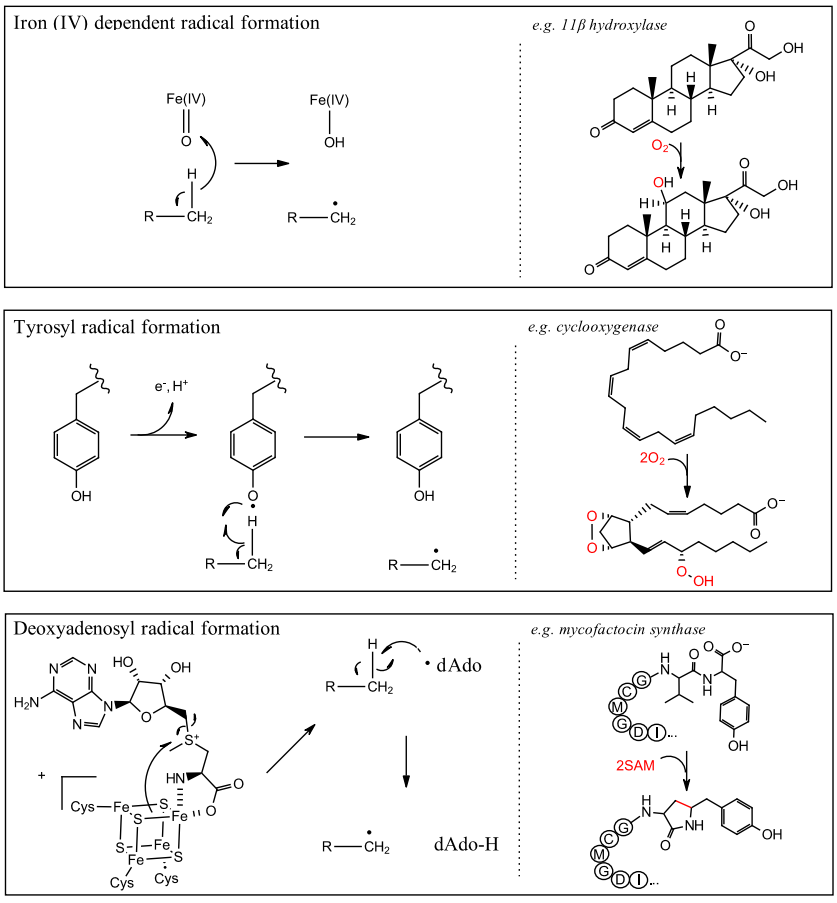

Figure A.2: *Generic reaction schemes showing the canonical iron catalyzed radical rebound reaction, the oxidation of tyrosine to form the tyrosyl radical, and the homolytic cleavage of S-adenosylmethionine to form the 5'-deoxyadenosyl radical (•dAdo). Biologically relevant examples that use the respective reactions are shown on the right. They include the hydroxylation of sterol to cortisol, oxidation and cyclization of arachidonic acid, and the cyclization of the mycofactocin peptide MftA.*

Kinetic Isotope Effects as Mechanistic Probes of C-H Activation

C-H activation can involve proton (H^+), hydrogen atom (H•), or hydride (H^-) transfer. These processes can be described using kinetic isotope effects (KIEs), which, in general, are the ratio of the rate constant for a light isotope (k_L), such as protium, over the rate constant for a heavy isotope, (k_H), such as deuterium:

$$KIE = \frac{k_L}{k_H} \quad (1)$$

KIE measurements are routinely used for the determination of rate determining steps and/or for the study of reaction mechanisms.[45] The KIE measured for the transferred particle is referred to as a primary KIE and its magnitude is dominated by the differences in zero-point energies (ZPE) in the ground state (**Figure A.3A**). For C-H bond cleavage, the reaction coordinate involves conversion of a vibrational stretch in the ground state to a translation in the transition state and, therefore, neglects isotopic ZPEs in the transition state. While isotopic substation of heavy atoms (e.g. $^{12}C/^{13}C$) can give rise to measurable effects, the largest primary KIEs observed and predicted are for the exchange of protium (^1H; 99.98 % abundance) for deuterium (^2H) or tritium (^3H). Secondary KIEs, measured with isotopically labeled atoms that are not involved in the bond that is being cleaved, can also be exploited for elucidating reaction mechanisms. The focus of this Chapter will be on the primary deuterium kinetic isotope effects on the first-order rate constant, $^Dk_{cat}$, collected under saturating substrate concentrations. For (partial) rate determining hydrogen transfer steps, observed primary hydrogen/deuterium KIEs are 'normal' (i.e. the rate for hydrogen transfer is greater than the rate for deuterium transfer) and have a large range of magnitudes as small as 1.5 to very elevated values (cf. **Table A.2**).[46–48] For comparison, secondary kinetic isotope effects can be normal or inverse (i.e. rate of deuterium transfer is faster than protium) and are generally small, <1.5.[49–51] In contrast to O-H or N-H bonds, the covalent nature of C-H bonds

permits the ability to stably exchange the naturally-occurring protium isotope for one of its heavier isotopes.

From the classical TST models of catalysis, the observation of a primary KIE can be explained by the quantization of energy in the chemical bonds. For simplicity, let's consider a chemical bond as two atoms attached by a spring. In this case, the particles experience a restoring force that is proportional to their displacement (x) by the force constant (F). Hooke's law, Eq (2), relates the frequency of motion (ν) to the reduced mass (μ) of the atoms undergoing oscillation, Eq (3), and the force constant characteristic of the bond. Force constants are the same for isotopic substitution and thus changes in vibrational frequency result from changes in μ:

$$\nu = \frac{1}{2\pi}\sqrt{\frac{F}{\mu}} \tag{2}$$

$$\mu = \frac{m_1 m_2}{m_1 + m_2} \tag{3}$$

In the case of carbon-hydrogen bonds, the stretching frequencies are calculated to be ν =3000 cm^{-1} (C–^{1}H), ν = 2200 cm^{-1} (C–^{2}H), and ν = 1800 cm^{-1} (C–^{3}H). The energy of a bound particle ($h\nu$) is defined by the harmonic-oscillator approximation according to Eq (4), where h is Planck's constant ($h = 6.626 \times 10^{-34}$ J s) and vibrational energy levels are designated n_{vib}. The zero-point energy ($n_{vib} = 0$) is the lowest vibrational energy level of a harmonic oscillator. These ZPEs dominate the origin of KIEs within a semi-classical picture:

$$E_{vib} = (n_{vib} + 1/2)h\nu, \quad n_{vib} = 0, 1, 2, \ldots \tag{4}$$

It follows that reduced mass differences cause the zero-point energies to follow a trend, C–^{1}H > C–^{2}H > C–^{3}H, as shown in **Figure A.3A**. The differences in the zero-point levels of the reactant state give the *upper limit* to the primary KIE through Eq (5), where the subscripts L and H

designate the lighter and heavier isotope, respectively. In the case of hydrogen transfer from carbon, the stretching frequencies of C–H bonds lead to estimates of primary KIEs of 7 and 18 for k^1_H/k^2_H and k^1_H/k^3_H at 298 K, respectively:

$$\frac{k_L}{k_H} = exp[(hv_H - hv_L)/2RT] \quad (5)$$

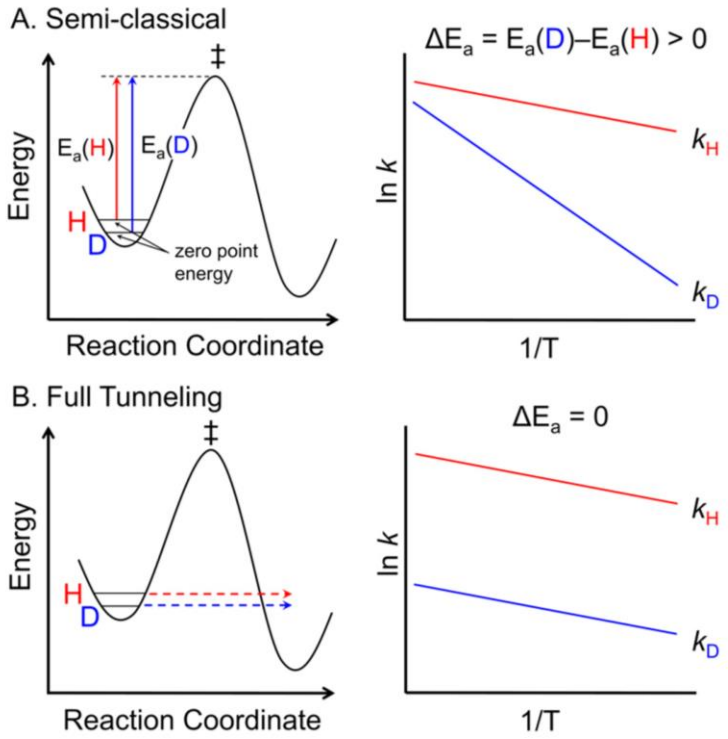

Figure A.3. *Reaction progress diagrams (left) and Arrhenius plots (right) for the cleavage of C-H/C-D bonds. Transition states are indicated by '‡'. A. Representation of semi-classical origins of the KIE. B. Representation of a full tunneling mechanism for hydrogen transfer through the barrier.*

Anomalous KIEs for Homolytic C-H Bond Cleavage

Although the upper limit of the semi-classical TST model primary deuterium KIE is 7, there are several cases in the literature of C-H activation reactions catalyzed by native enzymes that report primary deuterium KIEs of up to100 (**Table A.2**). One such family of enzymes, lipoxygenases, has routinely shown large KIEs across several organisms with isotope effects of ≥

40 for cleavage a singly labeled C-H bond. In a surprisingly extreme case, a mutant variant of the paradigmatic soybean lipoxygenase, L546A/L754A, exhibited an unprecedented KIE of ~660 at room temperature.[48]

Table A.2: *Examples of enzyme systems exhibiting primary deuterium KIEs, $^{D}k_{cat}$, and their temperature dependence (ΔE_a) values that deviate from semi-classical TST behavior*

Enzyme	**$^{D}k_{cat}$**	**ΔE_a (kcal/mol)**	**References**
Lipoxygenases (H•)	40-100	0-0.9	[52–55]
L546A/L754A Soybean lipoxygenase (H•)	~660	0.3 (0.7)	[48]
Methane monooxygenase (H•)	100	N.D.	[47]
TauD monooxygenase (H•)	37	N.D.	[56]
Fatty acid α-oxygenase (H•)	30-120	1.1 (0.3)	[57,58]
Methyl malonyl CoA mutase (H•)	36	N.D.	[59]
Cyclooxygenase-2	~20-30	0.1 ± 0.7	[60]
Galactose oxidase (H•)	16-32	N.D.	[61]
Acyl CoA desaturase (H•)	23	≤ 1	[62]
Methylamine dehydrogenase (H•)	13-17	~0	[63]
Peptidylglycine α-amidating monooxygenase (H•)	11	0.4	[64]
Thermophilic alcohol dehydrogenase (H^-)	1.5 (T>30ºC) 2-7 (T<30ºC)	ΔE_a ~ 0 (T>30ºC) ΔE_a >> 0 (T<30ºC)	[65]

Large $^{D}k_{cat}$ values, in excess of the limit from semi-classical TST, *can implicate* quantum (i.e. tunneling) effects associated with the transferred particle. However, not all C-H activation reactions catalyzed by enzymes are associated with 'deviant' KIEs. In the examples presented in **Table A.2**, anomalous $^{D}k_{cat}$ values arise from enzyme C-H activation reactions in which the C-H bond is cleaved via a homolytic mechanism (i.e. formal H• transfer; **Figure A.1**). In the cases of *heterolytic* C-H activation (H^+ or H^- transfer), observed KIEs are typically 'normal'.

One of the most well studied examples is that of the thermophilic alcohol dehydrogenase from *Bacillus stearothermophilus* (ht-ADH) which catalyzes the hydride transfer reaction from short chain alcohols to an NAD^+ cofactor.[65] As typically seen in extremophiles, ht-ADH exhibits a break from the expected linear trend in kinetic behavior as a function of temperature. Originating from a thermophile, ht-ADH has been evolved to function optimally at higher temperatures. At temperatures elevated from the break at 30ºC, the KIE (1.5) is normal, while below this break point, the kinetic isotope effects approach the theoretical limit for semi-classical transition state catalysis (**Table A.2**).[65] Based on the analysis of the KIEs alone, the ht-ADH reaction would not be expected to have a significant, if at all, quantum contribution.

While the magnitude of the KIE can be suggestive of quantum effects in enzyme catalysis, the temperature dependence of the kinetic isotope effect ($\Delta E_a = E_a(D) - E_a(H)$) has emerged as a vital kinetic parameter in revealing quantum tunneling effects in enzyme reactions.[66] For enzymatic C-H activation reactions with measured ΔE_a parameters (**Table A.2**), the values are equal to or nearly zero. This behavior contrasts ΔE_a values from semi-classical TST in which the activation energy for deuterium transfer is larger than that for protium transfer (i.e. $\Delta E_a > 0$) due to differences in their zero-point energies (**Figure A.3A**). As will be explained in more detail in ensuing sections, full tunneling models, in which the transferred hydrogen and its isotopes behave

as waves, can adequately explain ΔE_a values of (near) zero (cf. **Figure A.3B**). In the case of ht-ADH, the observation of ΔE_a values of ~0 above the break point (30ºC) is similar to that seen for H• transfer reactions.[65] It is now recognized that a wide range of KIEs, with values both larger and smaller than those predicted by Eq (5), are consistent with mechanisms of tunneling.

Quantum Effects for the Transfer of Electrons and Heavy Atoms

Electrons behave as both particles and waves. This wave-particle dualism[67] is so well known that it is often taught in high school physics classes. However, the transfer of atoms such as hydrogen with wavelike property is seldom (if at all) introduced and typically only described in the context of particle transfer. Atoms also have wavelengths, with this property dependent on the mass (m) and velocity (v) of the particle. Defining the unbound particle's kinetic energy as $E = (1/2\ mv^2)$ allows de Broglie wavelengths, λ_{dB}, to be calculated (**Table A.3**):

$$\lambda_{dB} = h/(2mE)^{1/2} \qquad (6)$$

When the electron is compared to hydrogen and to carbon, there is an extremely large variation in their quantum wavelengths, from 27 Å to 0.63 Å to 0.18 Å, respectively (**Table A.3**). The close correspondence between the computed de Broglie wavelengths for the electron and hydrogen to the distances traversed by these particles in chemical reactions is consistent with experimental findings that tunneling is operative within the functional temperature range of biological systems. This property also highlights that group transfer, such as that catalyzed by methyl transferases,[68] is not expected to be associated with a significant probability of a quantum contribution.

Table A.3. *de Broglie wavelengths of the electron and heavy atoms*

Particle	e^-	^1H	^2H	^3H	^{12}C
mass (amu)	1/1750	1	2	3	12
λ_{dB} (Å)	27	0.63	0.45	0.36	0.18

Tunneling Model for PCET

Following a series of theoretical efforts at the start of the 1950s, a new theory (Marcus-Hush theory) for the nature of electron transfer reactions emerged.[69] The resulting formalism rationalizes electron tunneling in the context of the Frank Condon principle: as the inner coordination shells of the donor and acceptor atom became more energetically similar, the electron transfer probability is enhanced. In other words, the transfer of electrons is dominated by their wavelike properties. The important implication is that there is no classical transition state and the kinetic barrier for such reactions is ascribed to the environmental reorganization energy, λ_{re} (**Figure A.4**).

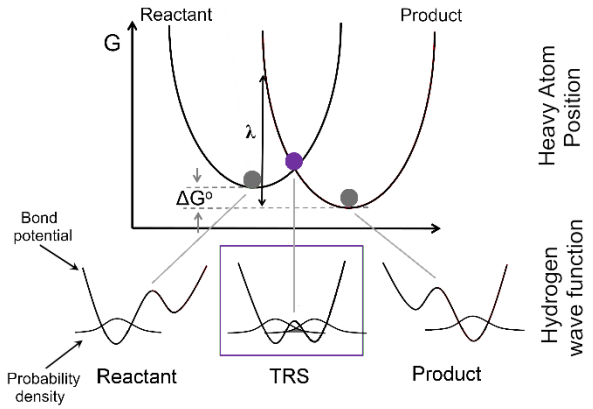

Figure A.4: *Graphical representation of the Marcus reaction coordinate involving the heavy atom positions and defined by λ_{re} and the driving force, ΔG^o. At the TRS (purple dot), the positioning of the hydrogenic wave function has become energetically degenerate across the donor and acceptor wells.*

λ_{re} represents the energetic cost associated with the geometric (distance and orientation) and electrostatic optimization of the donor and acceptor to form degeneracy (along the quantum coordinate) of the wave functions at the so-called tunneling-ready state (TRS). This process involves both inner-sphere (i.e. cofactor and reactant) and outer-sphere (i.e. solvent) contributions. In the case of enzymes, the latter will also include the protein itself. It follows that if minor optimization of the local geometries is needed (small λ_{re}), the transfer rate will be faster.

The emergence of extremely large primary kinetic isotope effects that are temperature independent supported the assignment of *through the barrier* (tunneling) mechanisms for biological C-H activation reactions. The current version of the vibronically non-adiabatic analytical expression for hydrogen transfer reflects the model developed to conceptualize electron transfer: protein or solvent fluctuations generate a reactive configuration along the classical, heavy-atom coordinate, from which the hydrogen transfers via a quantum (wave function) coordinate (**Figure A.4**). The barrier of the heavy atom coordinate is dependent on λ_{re} and the reaction free energy ΔG^{o}. The rate of hydrogen transfer will also depend on the electronic coupling and an isotopically dependent overlap between the reactant and product wave functions.

Because the de Broglie wavelength of hydrogen is much smaller than the electron, quantum mechanical hydrogen transfer is extremely sensitive to minor changes in distance. To account for the latter, an additional coordinate to Marcus expression is introduced that accounts for thermal sampling of the donor and acceptor distance to promote the probability of hydrogen wave function overlap (**Figure A.5)**. In natively evolved enzymes, both computational and experimental data support average donor acceptor distances (DADs) of 2.7 to 2.8 Å within a TRS in which the reactant and product hydrogenic wave functions have become degenerate (**Figure A.4, purple box**).[29] In these cases, the contribution of this DAD sampling coordinate is minimal (**Figure A.5**,

bottom). A different behavior emerges in reactions where the enzyme has been perturbed, as occurs via site-directed mutagenesis. In almost all such cases, there is an empirical increase in the kinetically resolved ΔE_a (**Figure A.5**, **top**). This phenomenon can be understood as a mutation-induced elongation of the DAD and increases the contribution of the DAD sampling.[66] Because of a less diffuse wave function for deuterium (**Table A.3**), the contribution of distance sampling is increased relative to protium (**Figure A.5**). As will be shown for the case study of SLO, single site mutations have been linked to ΔE_a as large as 5 kcal/mol, well in excess of the 1.2-2 kcal/mol limit by semi-classical TST.

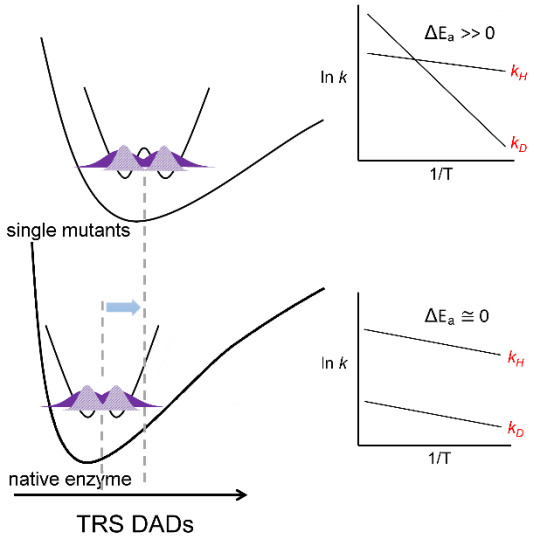

Figure A.5: *Left. Potential energy surfaces for the hydrogen wave function DAD sampling coordinate, formed at the TRS (**Figure A.4**, purple box), that influences the efficiency of wave function overlap. The ^1H (protium) and ^2H (deuterium) wave functions are represented as dark and light purple, respectively. Right. Arrhenius plots, determined from enzyme kinetics, for the cleavage of C-H/C-D bonds, highlighting the difference in experimental patterns between native enzymes ($\Delta E_a \sim 0$) and impaired, mutant enzymes ($\Delta E_a >> 0$). An increased ΔE_a arises from a disproportionate increase in thermal sampling for ^2H with respect to ^1H because the ^1H wave function overlap is attained upon mutation-induced elongation in DAD (top left), but the ^2H wave function overlap is compromised due to its shorter de Broglie wavelength (**Table A.3**). For the mutation effects (top), note how the Arrhenius behavior can also differ from that predicted for reactions with semi-classical transition states (cf. **Figure A.3A**).*

Important Implication towards Catalysis: Active Site Compaction and Protein Motions

The emerging view from studies of C-H activation by native enzymes is that the donor carbon and acceptor (typically oxygen) must come into close proximity (2.7-2.8 Å) for effective hydrogen wavefunction overlap, that is to say for efficient C-H bond cleavage.[29] The importance of this distance can be conceptualized by a cartoon representation of the particles in a classical treatment (**Figure A.6**). As indicated above, in comparison to the electron, the de Broglie wavelength of hydrogen is short (0.6-0.7 Å). From the point of view of quantum tunneling dominated catalysis, in order for the wavefunction overlap to occur, the center-of-mass distance between the positioning of hydrogen on the donor (carbon) and the hydrogen on the acceptor (oxygen) will be ~0.7 Å. Taking into account the bond lengths for carbon-hydrogen (1.09 Å) and oxygen-hydrogen (0.96 Å), the center-of-mass distance between carbon and oxygen must approach 2.7 Å (**Figure A.6**, **bottom**). It is clear from this distance that the van der Waals (vdW) surfaces of carbon and oxygen clash. This view of the TRS – the state at which hydrogen wavefunction is degenerate across donor and acceptor wells – contrasts that of the ground state geometries of the immediately formed ES complex, in which their internuclear (center-of-mass) distances between donor and acceptor are frequently observed with vdW contacts of ~3.2 Å.

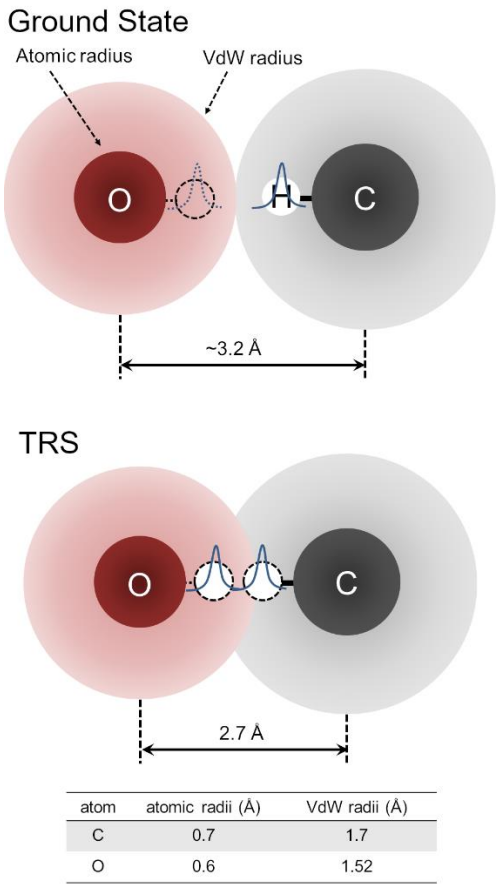

atom	atomic radii (Å)	VdW radii (Å)
C	0.7	1.7
O	0.6	1.52

Figure A.6: *Cartoon depiction of the ground state (top) and TRS (bottom) between the hydrogen donor, carbon, and acceptor, oxygen. For display purposes, the carbon-hydrogen bond (thick solid line) is shown in line with the acceptor. The hydrogen wave function probability on the donor is represented in 2-D by the blue curve. The corresponding positioning of the hydrogen atom (dashed circle), hydrogen-oxygen bond (dashed line), and wave function probability (dashed blue curve). The hydrogen-carbon bond length is 1.09 Å and the hydrogen-oxygen bond length is 0.96 Å. At the TRS, there is probability that the H atom is either on the carbon or oxygen atom. The atomic and vdW radii for carbon and oxygen are listed in the table. For simplicity purposes, attractive and repulsive forces are being ignored.*

This model of catalysis therefore implicates that the donor and acceptor atoms must become 'compacted' (or 'compressed'[70]) during the progression of the reaction coordinate to facilitate degenerate hydrogen wave function overlap across donor and acceptor wells. Because these reduced distances are not seen in the average ground state configuration of the ES complex, compaction must arise transiently from conformational sampling of the protein

Case study of C-H activation enzyme, soybean lipoxygenase

Lipoxygenases catalyze the regio- and stereo-specific insertion of molecular oxygen into polyunsaturated fatty acids. The resulting hydroperoxides serve as cell signaling mediators for a diverse range of physiological roles.[71] For instance, in humans, there are six isoforms of the enzymes that are involved in normal homeostasis and even in tumor suppression as well as linked to pro-inflammatory responses, such as stroke, diabetes, cancer, and heart disease.[72] In plants, these enzymes are pivotal for seed germination, growth and development, as well as pathogenic defense.[73] The roles of LOXs in fungi and prokaryotes are currently not known. While these enzymes are well represented across the kingdoms, the soybean lipoxygenase L-1 isoform (SLO) has served as the paradigm of the family in regards to developing the mechanistic understanding for enzymatic C-H activation reactions. The conserved mechanism for the oxidation of fatty acids by iron dependent lipoxygenases is shown in **Figure A.7**.[74] In the case of SLO, the preferred fatty acid substrate, linoleic acid (LA), binds into a long and primarily hydrophobic channel that places the reactive carbon of substrate proximal to a mononuclear, non-heme ferric hydroxide cofactor. The ferric hydroxide cofactor is responsible for hydrogen atom (formal H•) abstraction from carbon-11 of LA, generating a delocalized substrate-based radical that is subsequently quenched rapidly by oxygen across a wide range of oxygen concentrations.[75] From the large body of available experimental data,[74,76] the C-H bond cleavage step of SLO is rate-limiting and irreversible. Under saturating substrate concentrations, this step is associated with a large primary KIE of 80 (**Table A.4**) that is weakly temperature dependent (i.e ΔE_a = 0.9 kcal/mol), confirming a deep tunneling reaction mechanism (**Figure A.3B**). Further, the C-H bond cleavage step has been concluded to precede molecular oxygen insertion into the substrate radical via a channel that is

distinct from the substrate binding channel.[77] The oxygen channel provides the regio-specific nature of the hydroperoxide product.

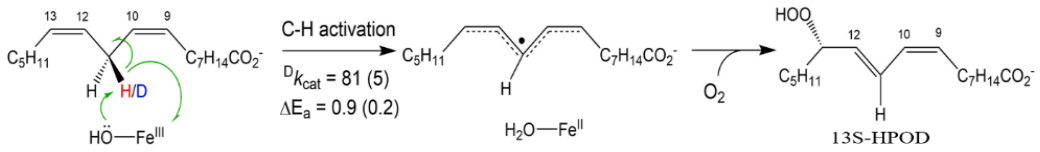

Figure A.7: *Reaction mechanism for the oxidation of LA by SLO. The first and rate-limiting step is C-H activation, in which the proton moves to the iron-bound hydroxide and the electron reduces Fe(III) to Fe(II).*

Important Implication towards Catalysis: Role of Hydrophobic Residues

SLO has served as an important example of how altering the size of hydrophobic side chains surrounding the substrate pocket can impact catalysis through measurable changes in the ΔE_a.[66,78,79] Three (nearly) invariant, aliphatic residues were identified from inspection of the high resolution (1.4 Å) X-ray crystal structure (**Figure A.8**). Two residues (L546 and L754) flank the position where the expected reactive carbon of substrate (carbon-11) resides and an addition residue (I553) that is distal from the cofactor site but is anticipated to contact the substrate. As shown in **Table A.2**, the simultaneous mutation of L546 and L754 to the volume-reducing alanine sidechain resulted in a 10,000-fold reduction in k_{cat} and an enormous KIE (~660).[48,80]

The I553X variants, where X = Ile, Val, Ala and Gly, however, exhibited modest changes in the values for k_{cat} and $^Dk_{cat}$, compared to the native enzyme. The most significant kinetic parameter to emerge from this mutational study was an increase in the ΔE_a from 0.9 kcal/mol in WT to 5.3 kcal/mol in I553G that mirrored the reduction in sidechain volume (**Figure A.9**). These data provide robust experimental support for the theoretical formalism that attributes increasing

ΔE_a values to packing defects within the active site. The consequences of packing defects are elongated DADs and increased donor-acceptor distance sampling thermal sampling that leads to a greater distance distribution. The latter the less diffuse ^2H wave function to a greater extent than ^1H; from a kinetic perspective, this physical property translates to a disproportionate increase in $E_a(D)$ in relation to $E_a(H)$ – in other words, an increase in the ΔE_a (**Figure A.5**).

Table A.4: *Kinetic parameters of wild-type (WT) vs. single site, second shell mutants of soybean lipoxygenase.*

SLO	k_{cat} (s^{-1})	E_a (kcal/mol)	$^{D}k_{cat}$	ΔE_a (kcal/mol)
WT[a]	297 (12)	2.1 (0.2)	81 (5)	0.9 (0.2)
I553L[b]	273 (10)	0.4 (0.7)	81 (3)	3.4 (0.6)
I553V[b]	91 (5)	2.4 (0.5)	77 (6)	2.6 (0.5)
I553A[a]	280 (10)	1.9 (0.2)	93 (4)	4.0 (0.3)
I553G[b]	58 (4)	0.03 (0.04)	178 (16)	5.3 (0.7)
L546A/L754A[c]	0.021 (0.001)	9.9 (0.2)	~660	0.3 (0.7)

[a]From reference[78]

[b]From reference[79]

[c]From reference[48]

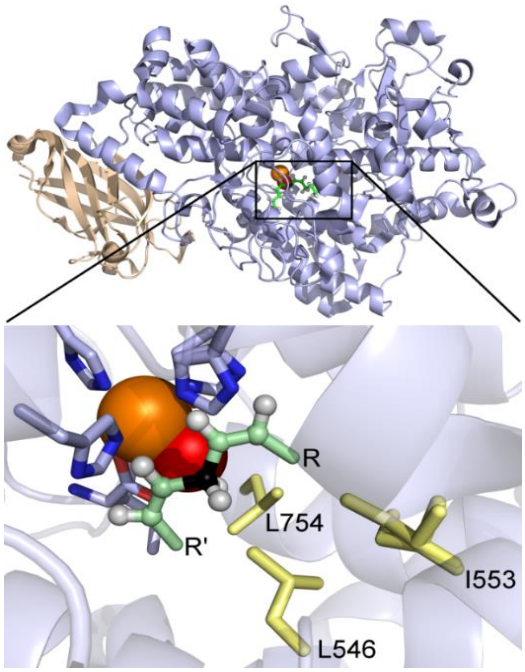

Figure A.8: *Structure of SLO and its active site. The two domains are color coded: wheat, N-terminal regulatory domain, and light blue, C-terminal catalytic domain. The reactive portion of the substrate linoleic acid, pale green, has been modeled into the high resolution X-ray structure of SLO (PDB: 3PZW) using experimentally-derived geometric constraints; the reactive carbon, C11, is colored black. Relevant aliphatic side chains are shown as pale-yellow sticks. The ferric hydroxide cofactor is displayed as orange and red spheres, respectively. Reproduced with permission from reference 29. Copyright 2017 JACS.*

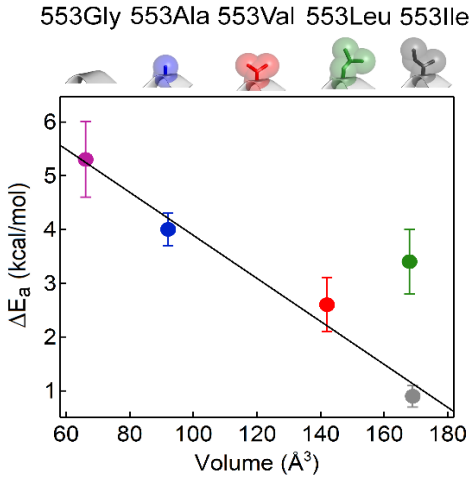

Figure A.9: *Kinetic-determined ΔE_a versus the volume of I553X. Reproduced with permission from reference.*[81] *Copyright 2020 Biochemistry.*

Origins of the Catalytic Activation Energy

The temperature dependence of enzyme catalysis (i.e. activation energy, E_a) is often challenging to interpret. Factors such as protein conformational changes/thermal melting or changes in rate-limiting steps can complicate the analysis. The observation of curvature effects in the Arrhenius plots has been attributed to changes in the specific heat capacity of proteins. Due to the fact that enzyme reactivity is typically limited to a narrow temperature range, the assignment of curvature in an Arrhenius plot is not always compelling.

Assuming that careful controls are explored to address these issues, a select few interpretations have emerged in the literature that provide a rationale for the empirical temperature dependence in the linear range of enzyme rate constants. Perhaps the most important, though the least cited, interpretation was provided by Tolman in the 1920's. Tolman claimed that the activation energy is the result of the difference in the total energy of all reactive states (E_{re}) relative to the total energy of all available states ($\bar{E}$):

$$E_a = E_{re} - \overline{E} \qquad (7)$$

This conceptualizes the empirical activation energy as an equilibrium effect and is therefore related to collisional theory.[82–84] How does this relate to enzyme reactions? The interpretation has been extended towards a conformational energy landscape.[85,86] While in some ways the conformational landscape is analogous to the energy landscape associated with protein folding,[87] the conformational landscape relevant to catalysis is linked to more subtle and stochastic fluctuations (i.e. randomized wiggling and jiggling). From this model, catalysis then results from the successful

achievement of a subset of uniquely competent conformations. In contrast to the 'induced fit' model, the catalytically-linked conformational sampling (landscape) is 'slaved' to the solvent.[88]

Important Implications towards Catalysis: Protein Thermal Networks

If the solvent-protein interactions are responsible for the temperature dependence of catalysis, then how is thermal energy transferred from the surface to buried, solvent-excluded active sites? Given the deep tunneling behavior in enzyme catalyzed C-H activation, as established for the SLO reaction, a second critical property emerged concerning the physical origins of the empirical temperature dependencies governing catalysis.

From Marcus theory, the probability of wavefunction overlap (**Figure 4**, bottom) is inherently temperature independent. Further, the C-H bond cleavage step from SLO, that is well modeled to this modified theory, is rate-determining and irreversible. Thus, the observed activation energy, E_a, *must originate from the reorganization of the enzyme-substrate complex*. This property enables us to provide a clear picture into how heat is transferred to activate catalysis when the active site is 'insulated' from solvent. In the case of SLO, the application of hydrogen-deuterium exchange (HDX) as a function of temperature provided the ability to spatially examine the thermodynamics of local protein fluctuations.[89] HDX reports on the exchange of peptidyl amide N-H to N-D when the protein is incubated in deuterium oxide as a function of time and temperature.

From the comparative analysis of the regional activation energies of HDX, $E_{a(HDX)}$, versus mutational impact on the activation energy from catalysis, E_a, a thermal conduit involving a nonconserved loop was identified (**Figure A.10**).[89] This spatial resolution study was expanded to temporal analysis using temperature dependent fluorescent Stokes shifts and the site-selective

incorporation of a blue-shifted fluorophore at position 322 (at the tip of the thermal loop).[90] A model for this behavior has been advanced in which collisions at the solvent:loop (including peptide 317–334) interface initiate thermal activation that is then transmitted toward the donor-acceptor pair, located 15–34 Å from the surface loop.

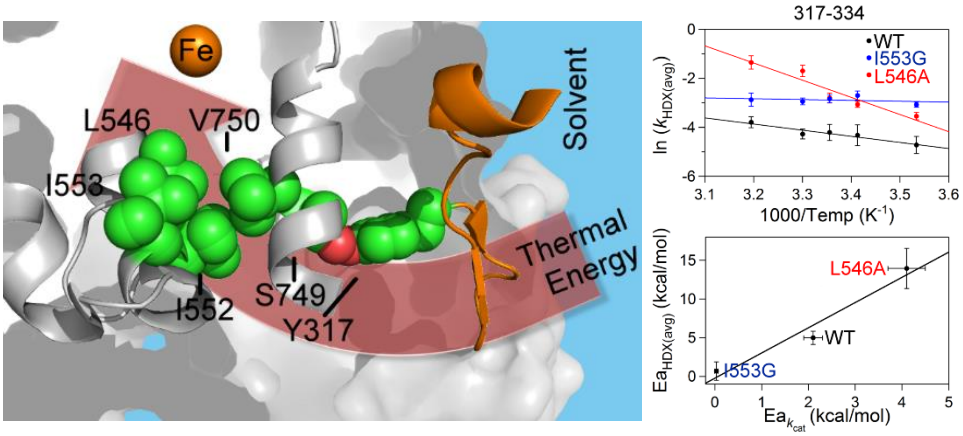

Figure A.10: *Diagram of the protein network in SLO that mediates thermal activation (left). This was determined from the impact of mutation on $E_a(k_{cat})$ for the rate limiting hydrogen transfer step in comparison to E_a(HDX) derived from spatially resolved hydrogen deuterium exchange experiments (right). The peptide, 317-334, is colored orange on the SLO model. Reproduced with permission from reference 89. Copyright 2017 ACS Central Science.*

Such proteins networks have also been implicated in the tetrameric C-H activation enzyme, alcohol dehydrogenase.[91–93] These findings provide experimental evidence for thermally induced "protein quakes"[90] as the origin of enthalpic barriers in C-H activation catalysis.

Concluding remarks and path forward

The awesome catalytic power of natural enzymes coupled with the emergence of only a select few man-made '*de novo* enzymes' to match the benchmarks of moderately proficient enzymes, underscores the fact that the classical view of enzyme catalysis (i.e. transition state

stabilization) is not the complete picture of how enzymes work. In this Chapter, several important implications for enzyme-catalyzed C-H activation reactions have been presented:

1) Active site compaction
2) Involvement of protein motions to promote wave function overlap
3) Importance of hydrophobic residues to facilitate substrate positioning
4) Discrete protein networks for thermal activation of catalysis

Considering that the few successful examples of *de novo* enzymes require several (8-16) rounds of directed evolution (i.e. randomized mutagenesis) and are often achieved through mutations at remote sites from the active site, elaboration of the above listed principles may ultimately allow us to expand the guidelines for the design of *de novo* catalysts towards C-H activation reactions that constitute a significant number of biologically and industrially relevant chemical transformations. The outlined guidelines above were developed through rigorous kinetic isotope effect studies coupled with biophysical tools including X-ray crystallography, hydrogen-deuterium exchange (HDX), and time-resolved spectroscopic methods. Such mechanistic strategies are expected to provide important information into designed (or redesigned)[94] enzyme reactions to identify the rate limiting steps of catalysis and to guide the incorporation of these additional catalytic features to help overcome the current barriers.[95]

References

(1) Wolfenden, R.; Snider, M. J. The Depth of Chemical Time and the Power of Enzymes as Catalysts. *Acc. Chem. Res.* **2001**, *34* (12). https://doi.org/10.1021/ar000058i.

(2) Radzicka, A.; Wolfenden, R. A Proficient Enzyme. *Science (80-.).* **1995**, *267* (5194). https://doi.org/10.1126/science.7809611.

(3) Miller, B. G.; Wolfenden, R. Catalytic Proficiency: The Unusual Case of OMP Decarboxylase. *Annual Review of Biochemistry*. 2002. https://doi.org/10.1146/annurev.biochem.71.110601.135446.

(4) Edwards, D. R.; Lohman, D. C.; Wolfenden, R. Catalytic Proficiency: The Extreme Case of S-O Cleaving Sulfatases. *J. Am. Chem. Soc.* **2012**, *134* (1). https://doi.org/10.1021/ja208827q.

(5) Pauling, L. Nature of Forces between Large Molecules of Biological Interest. *Nature* **1948**, *161* (4097). https://doi.org/10.1038/161707a0.

(6) Schultz, P. G. Catalytic Antibodies. *Angewandte Chemie International Edition in English*. 1989. https://doi.org/10.1002/anie.198912833.

(7) Lerner, R. A.; Benkovic, S. J.; Schultz, P. G. At the Crossroads of Chemistry and Immunology: Catalytic Antibodies. *Science (80-.).* **1991**, *252* (5006). https://doi.org/10.1126/science.2024118.

(8) Rohl, C. A.; Strauss, C. E. M.; Misura, K. M. S.; Baker, D. Protein Structure Prediction Using Rosetta. *Methods Enzymol.* **2004**, *383*. https://doi.org/10.1016/S0076-

6879(04)83004-0.

(9) Jiang, L.; Althoff, E. A.; Clemente, F. R.; Doyle, L.; Röthlisberger, D.; Zanghellini, A.; Gallaher, J. L.; Betker, J. L.; Tanaka, F.; Barbas, C. F.; Hilvert, D.; Houk, K. N.; Stoddard, B. L.; Baker, D. De Novo Computational Design of Retro-Aldol Enzymes. *Science (80-.).* **2008**, *319* (5868). https://doi.org/10.1126/science.1152692.

(10) Siegel, J. B.; Zanghellini, A.; Lovick, H. M.; Kiss, G.; Lambert, A. R.; St.Clair, J. L.; Gallaher, J. L.; Hilvert, D.; Gelb, M. H.; Stoddard, B. L.; Houk, K. N.; Michael, F. E.; Baker, D. Computational Design of an Enzyme Catalyst for a Stereoselective Bimolecular Diels-Alder Reaction. *Science (80-.).* **2010**, *329* (5989). https://doi.org/10.1126/science.1190239.

(11) Röthlisberger, D.; Khersonsky, O.; Wollacott, A. M.; Jiang, L.; DeChancie, J.; Betker, J.; Gallaher, J. L.; Althoff, E. A.; Zanghellini, A.; Dym, O.; Albeck, S.; Houk, K. N.; Tawfik, D. S.; Baker, D. Kemp Elimination Catalysts by Computational Enzyme Design. *Nature* **2008**, *453* (7192). https://doi.org/10.1038/nature06879.

(12) Giger, L.; Caner, S.; Obexer, R.; Kast, P.; Baker, D.; Ban, N.; Hilvert, D. Evolution of a Designed Retro-Aldolase Leads to Complete Active Site Remodeling. *Nat. Chem. Biol.* **2013**, *9* (8). https://doi.org/10.1038/nchembio.1276.

(13) Obexer, R.; Godina, A.; Garrabou, X.; Mittl, P. R. E.; Baker, D.; Griffiths, A. D.; Hilvert, D. Emergence of a Catalytic Tetrad during Evolution of a Highly Active Artificial Aldolase. *Nat. Chem.* **2017**, *9* (1). https://doi.org/10.1038/nchem.2596.

(14) Eggerer, H. Covalent Catalysis by Enzymes. Von L. B. Spector. Springer-Verlag, Berlin 1982. XII, 276 S., Geb. DM 78.00. *Angew. Chemie* **2006**, *95* (10).

https://doi.org/10.1002/ange.19830951041.

(15) Zhang, X.; Houk, K. N. Why Enzymes Are Proficient Catalysts: Beyond the Pauling Paradigm. *Acc. Chem. Res.* **2005**, *38* (5). https://doi.org/10.1021/ar040257s.

(16) Cleland, W. W.; Kreevoy, M. M. Low-Barrier Hydrogen Bonds and Enzymic Catalysis. *Science (80-.).* **1994**, *264* (5167). https://doi.org/10.1126/science.8009219.

(17) Warshel, A.; Sharma, P. K.; Kato, M.; Xiang, Y.; Liu, H.; Olsson, M. H. M. Electrostatic Basis for Enzyme Catalysis. *Chemical Reviews*. 2006. https://doi.org/10.1021/cr0503106.

(18) Fried, S. D.; Bagchi, S.; Boxer, S. G. Extreme Electric Fields Power Catalysis in the Active Site of Ketosteroid Isomerase. *Science (80-.).* **2014**, *346* (6216). https://doi.org/10.1126/science.1259802.

(19) Jencks, B. W. P. BINDING ENERGY , SPECIFICITY , A N D ENZYMIC CATALYSIS : T H E CIRCE EFFECT. **1975**, *43*.

(20) Dewar, M. J. S.; Storch, D. M. Alternative View of Enzyme Reactions. *Proc. Natl. Acad. Sci. U. S. A.* **1985**, *82* (8). https://doi.org/10.1073/pnas.82.8.2225.

(21) WESTHEIMER, F. H. Mechanisms Related to Enzyme Catalysis. *Adv. Enzyme Regul.* **1962**, *24*. https://doi.org/10.1002/9780470124888.ch9.

(22) Fersht, A. *Structure and Mechanism in Protein Science*; 1999; Vol. 13409.

(23) Bruice, T. C. A View at the Millennium: The Efficiency of Enzymatic Catalysis. *Acc. Chem. Res.* **2002**, *35* (3). https://doi.org/10.1021/ar0001665.

(24) Brocchieri, L.; Karlin, S. Protein Length in Eukaryotic and Prokaryotic Proteomes. *Nucleic Acids Res.* **2005**, *33* (10). https://doi.org/10.1093/nar/gki615.

(25) Koshland, D. E. Correlation of Structure and Function in Enzyme Action. *Science (80-.).* **1963**, *142* (3599). https://doi.org/10.1126/science.142.3599.1533.

(26) Thoma, J. A.; Koshland, D. E. Competitive Inhibition by Substrate during Enzyme Action. Evidence for the Induced-Fit Theory. *J. Am. Chem. Soc.* **1960**, *82* (13). https://doi.org/10.1021/ja01498a025.

(27) Cha, Y.; Murray, C. J.; Klinman, J. P. Hydrogen Tunneling in Enzyme Reactions. *Science (80-.).* **1989**, *243* (4896). https://doi.org/10.1126/science.2646716.

(28) Klinman, J. P. An Integrated Model for Enzyme Catalysis Emerges from Studies of Hydrogen Tunneling. *Chem. Phys. Lett.* **2009**, *471* (4–6). https://doi.org/10.1016/j.cplett.2009.01.038.

(29) Klinman, J. P.; Offenbacher, A. R.; Hu, S. Origins of Enzyme Catalysis: Experimental Findings for C-H Activation, New Models, and Their Relevance to Prevailing Theoretical Constructs. *Journal of the American Chemical Society*. 2017. https://doi.org/10.1021/jacs.7b08418.

(30) Miller, W. H. Quantum Mechanical Transition State Theory and a New Semiclassical Model for Reaction Rate Constants. *J. Chem. Phys.* **1974**, *61* (5). https://doi.org/10.1063/1.1682181.

(31) Truhlar, D. G.; Hase, W. L.; Hynes, J. T. Current Status of Transition-State Theory. *J. Phys. Chem.* **1983**, *87* (15). https://doi.org/10.1021/j100238a003.

(32) Crabtree, R. H. Organometallic Alkane CH Activation. *Journal of Organometallic Chemistry*. 2004. https://doi.org/10.1016/j.jorganchem.2004.07.034.

(33) Stone, K. L.; Borovik, A. S. Lessons from Nature: Unraveling Biological C–H Bond Activation. *Current Opinion in Chemical Biology*. 2009. https://doi.org/10.1016/j.cbpa.2009.02.008.

(34) Bollinger, J. M.; Broderick, J. B. Frontiers in Enzymatic C-H-Bond Activation. *Current Opinion in Chemical Biology*. 2009. https://doi.org/10.1016/j.cbpa.2009.03.018.

(35) Brash, A. R. Lipoxygenases: Occurrence, Functions, Catalysis, and Acquisition of Substrate. *Journal of Biological Chemistry*. 1999. https://doi.org/10.1074/jbc.274.34.23679.

(36) Huang, X.; Groves, J. T. Beyond Ferryl-Mediated Hydroxylation: 40 Years of the Rebound Mechanism and C–H Activation. *Journal of Biological Inorganic Chemistry*. 2017. https://doi.org/10.1007/s00775-016-1414-3.

(37) Bauerle, M. R.; Schwalm, E. L.; Booker, S. J. Mechanistic Diversity of Radical S-Adenosylmethionine (SAM)-Dependent Methylation. *Journal of Biological Chemistry*. 2015. https://doi.org/10.1074/jbc.R114.607044.

(38) Fuchs, S. W.; Lackner, G.; Morinaka, B. I.; Morishita, Y.; Asai, T.; Riniker, S.; Piel, J. A Lanthipeptide-like N-Terminal Leader Region Guides Peptide Epimerization by Radical SAM Epimerases: Implications for RiPP Evolution. *Angew. Chemie - Int. Ed.* **2016**, *55* (40). https://doi.org/10.1002/anie.201602863.

(39) Khaliullin, B.; Ayikpoe, R.; Tuttle, M.; Latham, J. A. Mechanistic Elucidation of the Mycofactocin-Biosynthetic Radical S-Adenosylmethionine Protein, MftC. *J. Biol. Chem.* **2017**, *292* (31). https://doi.org/10.1074/jbc.M117.795682.

(40) Barr, I.; Latham, J. A.; Iavarone, A. T.; Chantarojsiri, T.; Hwang, J. D.; Klinman, J. P. Demonstration That the Radical S-Adenosylmethionine (SAM) Enzyme PqqE Catalyzes de Novo Carbon-Carbon Cross-Linking within a Peptide Substrate PqqA in the Presence of the Peptide Chaperone PqqD. *J. Biol. Chem.* **2016**, *291* (17). https://doi.org/10.1074/jbc.C115.699918.

(41) Schramma, K. R.; Bushin, L. B.; Seyedsayamdost, M. R. Structure and Biosynthesis of a Macrocyclic Peptide Containing an Unprecedented Lysine-to-Tryptophan Crosslink. *Nat. Chem.* **2015**, *7* (5). https://doi.org/10.1038/nchem.2237.

(42) Nakai, T.; Ito, H.; Kobayashi, K.; Takahashi, Y.; Hori, H.; Tsubaki, M.; Tanizawa, K.; Okajima, T. The Radical S-Adenosyl-L-Methionine Enzyme QhpD Catalyzes Sequential Formation of Intra-Protein Sulfur-to-Methylene Carbon Thioether Bonds. *J. Biol. Chem.* **2015**, *290* (17). https://doi.org/10.1074/jbc.M115.638320.

(43) Hudson, G. A.; Burkhart, B. J.; DiCaprio, A. J.; Schwalen, C. J.; Kille, B.; Pogorelov, T. V.; Mitchell, D. A. Bioinformatic Mapping of Radical S-Adenosylmethionine-Dependent Ribosomally Synthesized and Post-Translationally Modified Peptides Identifies New Cα, Cβ, and Cγ-Linked Thioether-Containing Peptides. *J. Am. Chem. Soc.* **2019**, *141* (20). https://doi.org/10.1021/jacs.9b01519.

(44) Denisov, I. G.; Makris, T. M.; Sligar, S. G.; Schlichting, I. Structure and Chemistry of Cytochrome P450. *Chemical Reviews*. 2005. https://doi.org/10.1021/cr0307143.

(45) Kohen, A. Kinetic Isotope Effects as Probes for Hydrogen Tunneling, Coupled Motion and Dynamics Contributions to Enzyme Catalysis. *Prog. React. Kinet. Mech.* **2003**, *28* (2). https://doi.org/10.3184/007967403103165486.

(46) Westheimer, F. H. The Magnitude of the Primary Kinetic Isotope Effect for Compounds of Hydrogen and Deuterium. *Chem. Rev.* **1961**, *61* (3). https://doi.org/10.1021/cr60211a004.

(47) Nesheim, J. C.; Lipscomb, J. D. Large Kinetic Isotope Effects in Methane Oxidation Catalyzed by Methane Monooxygenase: Evidence for C-H Bond Cleavage in a Reaction Cycle Intermediate. *Biochemistry* **1996**, *35* (31). https://doi.org/10.1021/bi960596w.

(48) Hu, S.; Soudackov, A. V.; Hammes-Schiffer, S.; Klinman, J. P. Enhanced Rigidification within a Double Mutant of Soybean Lipoxygenase Provides Experimental Support for Vibronically Nonadiabatic Proton-Coupled Electron Transfer Models. *ACS Catal.* **2017**, *7* (5). https://doi.org/10.1021/acscatal.7b00688.

(49) Cook, P. F.; Oppenheimer, N. J.; Cleland, W. W. Secondary Deuterium and Nitrogen-15 Isotope Effects in Enzyme-Catalyzed Reactions. Chemical Mechanism of Liver Alcohol Dehydrogenase. *Biochemistry* **1981**, *20* (7). https://doi.org/10.1021/bi00510a016.

(50) Anslyn, E. V. *Modern Physical Organic Chemistry*; Books, U. S., Ed.; Sausalito, California, 2006.

(51) Meyer, M. P.; Klinman, J. P. Investigating Inner-Sphere Reorganization via Secondary Kinetic Isotope Effects in the C-H Cleavage Reaction Catalyzed by Soybean Lipoxygenase: Tunneling in the Substrate Backbone as Well as the Transferred Hydrogen. *J. Am. Chem. Soc.* **2011**, *133* (3). https://doi.org/10.1021/ja1050742.

(52) Glickman, M. H.; Klinman, J. P. Nature of Rate-Limiting Steps in the Soybean Lipoxygenase-1 Reaction. *Biochemistry* **1995**, *34* (43). https://doi.org/10.1021/bi00043a013.

(53) Lewis, E. R.; Johansen, E.; Holman, T. R. Large Competitive Kinetic Isotope Effects in Human 15-Lipoxygenase Catalysis Measured by a Novel HPLC Method [9]. *Journal of the American Chemical Society*. 1999. https://doi.org/10.1021/ja983083g.

(54) Carr, C. A. M.; Klinman, J. P. Hydrogen Tunneling in a Prokaryotic Lipoxygenase. *Biochemistry* **2014**, *53* (14). https://doi.org/10.1021/bi500070q.

(55) Kostenko, A.; Ray, K.; Iavarone, A. T.; Offenbacher, A. R. Kinetic Characterization of the C-H Activation Step for the Lipoxygenase from the Pathogenic Fungus Magnaporthe Oryzae: Impact of N-Linked Glycosylation. *Biochemistry* **2019**, *58* (29). https://doi.org/10.1021/acs.biochem.9b00467.

(56) Price, J. C.; Barr, E. W.; Glass, T. E.; Krebs, C.; Bollinger, J. M. Evidence for Hydrogen Abstraction from C1 of Taurine by the High-Spin Fe(IV) Intermediate Detected during Oxygen Activation by Taurine:α -Ketoglutarate Dioxygenase (TauD). *J. Am. Chem. Soc.* **2003**, *125* (43). https://doi.org/10.1021/ja037400h.

(57) Gupta, A.; Mukherjee, A.; Matsui, K.; Roth, J. P. Evidence for Protein Radical-Mediated Nuclear Tunneling in Fatty Acid α-Oxygenase. *J. Am. Chem. Soc.* **2008**, *130* (34). https://doi.org/10.1021/ja8042273.

(58) Mukherjee, A.; Angeles-Boza, A. M.; Huff, G. S.; Roth, J. P. Catalytic Mechanism of a Heme and Tyrosyl Radical-Containing Fatty Acid α-(Di)Oxygenase. *J. Am. Chem. Soc.* **2011**, *133* (2). https://doi.org/10.1021/ja104180v.

(59) Chowdhury, S.; Banerjee, R. Evidence for Quantum Mechanical Tunneling in the Coupled Cobalt-Carbon Bond Homolysis-Substrate Radical Generation Reaction Catalyzed by Methylmalonyl-CoA Mutase [16]. *Journal of the American Chemical Society*. 2000.

https://doi.org/10.1021/ja994302g.

(60) Danish, H. H.; Doncheva, I. S.; Roth, J. P. Hydrogen Tunneling Steps in Cyclooxygenase-2 Catalysis. *J. Am. Chem. Soc.* **2011**, *133* (40). https://doi.org/10.1021/ja2059523.

(61) Whittaker, M. M.; Ballou, D. P.; Whittaker, J. W. Kinetic Isotope Effects as Probes of the Mechanism of Galactose Oxidase. *Biochemistry* **1998**, *37* (23). https://doi.org/10.1021/bi980328t.

(62) Buist, P. H.; Behrouzian, B. Use of Deuterium Kinetic Isotope Effects to Probe the Cryptoregiochemistry of Δ9 Desaturation. *J. Am. Chem. Soc.* **1996**, *118* (26). https://doi.org/10.1021/ja953262n.

(63) Basran, J.; Sutcliffe, M. J.; Scrutton, N. S. Enzymatic H-Transfer Requires Vibration-Driven Extreme Tunneling. *Biochemistry* **1999**, *38* (10). https://doi.org/10.1021/bi982719d.

(64) Francisco, W. A.; Knapp, M. J.; Blackburn, N. J.; Klinman, J. P. Hydrogen Tunneling in Peptidylglycine α-Hydroxylating Monooxygenase. *J. Am. Chem. Soc.* **2002**, *124* (28). https://doi.org/10.1021/ja025758s.

(65) Kohen, A.; Cannio, R.; Bartoluccl, S.; Klinman, J. P. Enzyme Dynamics and Hydrogen Tunnelling in a Thermophilic Alcohol Dehydrogenase. *Nature* **1999**, *399* (6735). https://doi.org/10.1038/20981.

(66) Klinman, J. P.; Offenbacher, A. R. Understanding Biological Hydrogen Transfer Through the Lens of Temperature Dependent Kinetic Isotope Effects. *Acc. Chem. Res.* **2018**, *51* (9). https://doi.org/10.1021/acs.accounts.8b00226.

(67) Greenberger, D. M. The Wave – Particle Dualism—A Tribute to Louis de Broglie on His

Ninetieth Birthday . *Am. J. Phys.* **1986**, *54* (2). https://doi.org/10.1119/1.14667.

(68) Zhang, J.; Klinman, J. P. Enzymatic Methyl Transfer: Role of an Active Site Residue in Generating Active Site Compaction That Correlates with Catalytic Efficiency. *J. Am. Chem. Soc.* **2011**, *133* (43). https://doi.org/10.1021/ja207467d.

(69) Marcus, R. A. On the Theory of Oxidation-Reduction Reactions Involving Electron Transfer. I. *J. Chem. Phys.* **1956**, *24* (5). https://doi.org/10.1063/1.1742723.

(70) Hay, S.; Pudney, C. R.; McGrory, T. A.; Pang, J.; Sutcliffe, M. J.; Scrutton, N. S. Barrier Compression Enhances an Enzymatic Hydrogen-Transfer Reaction. *Angew. Chemie - Int. Ed.* **2009**, *48* (8). https://doi.org/10.1002/anie.200805502.

(71) Liavonchanka, A.; Feussner, I. Lipoxygenases: Occurrence, Functions and Catalysis. *J. Plant Physiol.* **2006**, *163* (3). https://doi.org/10.1016/j.jplph.2005.11.006.

(72) Haeggstrom, J. Z.; Funk, C. D. Lipoxygenases and Leukotriene Pathways: Biochemistry, Biology, and Roles in Disease. *Chem. Rev.* **2011**, *111*, 5866–5898.

(73) Siedow, J. N. Plant Lipoxygenase: Structure and Function. *Annu. Rev. Plant Physiol. Plant Mol. Biol.* **1991**, *42* (1). https://doi.org/10.1146/annurev.pp.42.060191.001045.

(74) Klinman, J. P. Importance of Protein Dynamics during Enzymatic C-H Bond Cleavage Catalysis. *Biochemistry* **2013**, *52* (12). https://doi.org/10.1021/bi301504m.

(75) Knapp, M. J.; Klinman, J. P. Kinetic Studies of Oxygen Reactivity in Soybean Lipoxygenase-1. *Biochemistry* **2003**, *42* (39). https://doi.org/10.1021/bi0300884.

(76) Hatcher, E.; Soudackov, A. V.; Hammes-Schiffer, S. Proton-Coupled Electron Transfer in Soybean Lipoxygenase. *J. Am. Chem. Soc.* **2004**, *126* (18).

https://doi.org/10.1021/ja039606o.

(77) Collazo, L.; Klinman, J. P. Control of the Position of Oxygen Delivery in Soybean Lipoxygenase-1 by Amino Acid Side Chains within a Gas Migration Channel. *J. Biol. Chem.* **2016**, *291* (17). https://doi.org/10.1074/jbc.M115.709154.

(78) Knapp, M. J.; Rickert, K.; Klinman, J. P. Temperature-Dependent Isotope Effects in Soybean Lipoxygenase-1: Correlating Hydrogen Tunneling with Protein Dynamics. *J. Am. Chem. Soc.* **2002**, *124* (15). https://doi.org/10.1021/ja012205t.

(79) Meyer, M. P.; Tomchick, D. R.; Klinman, J. P. Enzyme Structure and Dynamics Affect Hydrogen Tunneling: The Impact of a Remote Side Chain (I553) in Soybean Lipoxygenase-1. *Proc. Natl. Acad. Sci. U. S. A.* **2008**, *105* (4). https://doi.org/10.1073/pnas.0710643105.

(80) Hu, S.; Sharma, S. C.; Scouras, A. D.; Soudackov, A. V.; Carr, C. A. M.; Hammes-Schiffer, S.; Alber, T.; Klinman, J. P. Extremely Elevated Room-Temperature Kinetic Isotope Effects Quantify the Critical Role of Barrier Width in Enzymatic C-H Activation. *J. Am. Chem. Soc.* **2014**, *136* (23). https://doi.org/10.1021/ja502726s.

(81) Offenbacher, A. R.; Sharma, A.; Doan, P. E.; Klinman, J. P.; Hoffman, B. M. The Soybean Lipoxygenase-Substrate Complex: Correlation between the Properties of Tunneling-Ready States and ENDOR-Detected Structures of Ground States. *Biochemistry* **2020**, *59* (7). https://doi.org/10.1021/acs.biochem.9b00861.

(82) Tolman, R. C. On the Derivation of the Equation for the Effect of Temperature on Reaction Rate. *J. Am. Chem. Soc.* **1925**, *47* (11). https://doi.org/10.1021/ja01688a006.

(83) Tolman, R. C.; Yost, D. M.; Dickinson, R. G. On Chemical Activation by Collisions. *Proc.*

Natl. Acad. Sci. **1927**, *13* (4). https://doi.org/10.1073/pnas.13.4.188.

(84) Truhlar, D. G. Interpretation of the Activation Energy. *J. Chem. Educ.* **1978**, *54* (5). https://doi.org/10.1021/ed055p309.

(85) Henzler-Wildman, K.; Kern, D. Dynamic Personalities of Proteins. *Nature*. 2007. https://doi.org/10.1038/nature06522.

(86) Benkovic, S. J.; Hammes, G. G.; Hammes-Schiffer, S. Free-Energy Landscape of Enzyme Catalysis. *Biochemistry* **2008**, *47* (11). https://doi.org/10.1021/bi800049z.

(87) Onuchic, J. N.; Luthey-Schulten, Z.; Wolynes, P. G. Theory of Protein Folding: The Energy Landscape Perspective. *Annu. Rev. Phys. Chem.* **1997**, *48* (1). https://doi.org/10.1146/annurev.physchem.48.1.545.

(88) Fenimore, P. W.; Frauenfelder, H.; McMahon, B. H.; Parak, F. G. Slaving: Solvent Fluctuations Dominate Protein Dynamics and Functions. *Proc. Natl. Acad. Sci. U. S. A.* **2002**, *99* (25). https://doi.org/10.1073/pnas.212637899.

(89) Offenbacher, A. R.; Hu, S.; Poss, E. M.; Carr, C. A. M.; Scouras, A. D.; Prigozhin, D. M.; Iavarone, A. T.; Palla, A.; Alber, T.; Fraser, J. S.; Klinman, J. P. Hydrogen-Deuterium Exchange of Lipoxygenase Uncovers a Relationship between Distal, Solvent Exposed Protein Motions and the Thermal Activation Barrier for Catalytic Proton-Coupled Electron Tunneling. *ACS Cent. Sci.* **2017**, *3* (6). https://doi.org/10.1021/acscentsci.7b00142.

(90) Zaragoza, J. P. T.; Nguy, A.; Minnetian, N.; Deng, Z.; Iavarone, A. T.; Offenbacher, A. R.; Klinman, J. P. Detecting and Characterizing the Kinetic Activation of Thermal Networks in Proteins: Thermal Transfer from a Distal, Solvent-Exposed Loop to the Active Site in

Soybean Lipoxygenase. *J. Phys. Chem. B* **2019**, *123* (41). https://doi.org/10.1021/acs.jpcb.9b07228.

(91) Liang, Z. X.; Lee, T.; Resing, K. A.; Ahn, N. G.; Klinman, J. P. Thermal-Activated Protein Mobility and Its Correlation with Catalysis in Thermophilic Alcohol Dehydrogenase. *Proc. Natl. Acad. Sci. U. S. A.* **2004**, *101* (26). https://doi.org/10.1073/pnas.0403337101.

(92) Meadows, C. W.; Balakrishnan, G.; Kier, B. L.; Spiro, T. G.; Klinman, J. P. Temperature-Jump Fluorescence Provides Evidence for Fully Reversible Microsecond Dynamics in a Thermophilic Alcohol Dehydrogenase. *J. Am. Chem. Soc.* **2015**, *137* (32). https://doi.org/10.1021/jacs.5b04413.

(93) Vaughn, M. B.; Zhang, J.; Spiro, T. G.; Dyer, R. B.; Klinman, J. P. Activity-Related Microsecond Dynamics Revealed by Temperature-Jump Förster Resonance Energy Transfer Measurements on Thermophilic Alcohol Dehydrogenase. *J. Am. Chem. Soc.* **2018**, *140* (3). https://doi.org/10.1021/jacs.7b12369.

(94) Renata, H.; Wang, Z. J.; Arnold, F. H. Expanding the Enzyme Universe: Accessing Non-Natural Reactions by Mechanism-Guided Directed Evolution. *Angewandte Chemie - International Edition*. 2015. https://doi.org/10.1002/anie.201409470.

(95) Baker, D. An Exciting but Challenging Road Ahead for Computational Enzyme Design. *Protein Science*. 2010. https://doi.org/10.1002/pro.481.

Appendix B: HDX Traces of wt *Mo*LOX and Glycosylation Variants

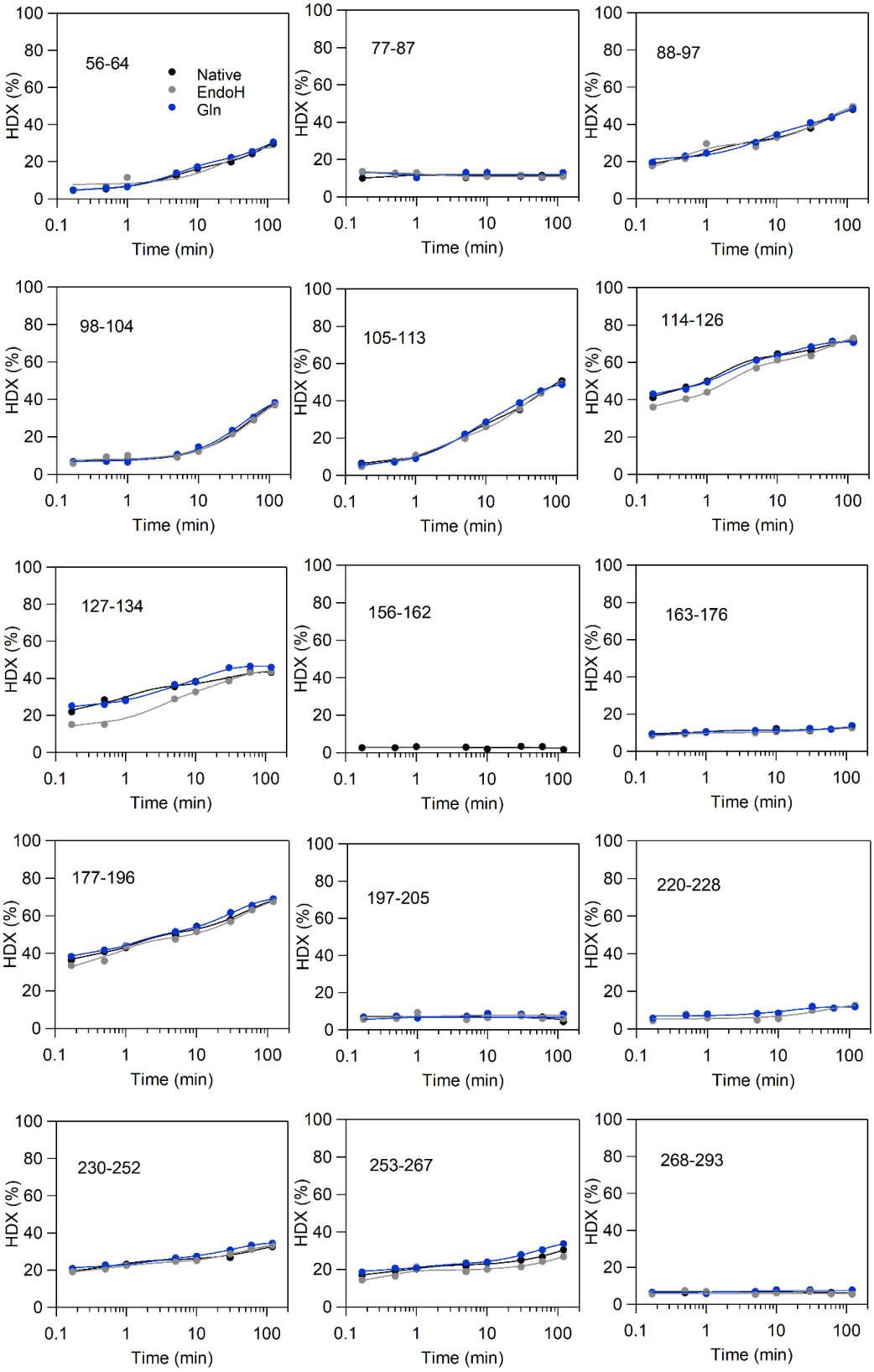

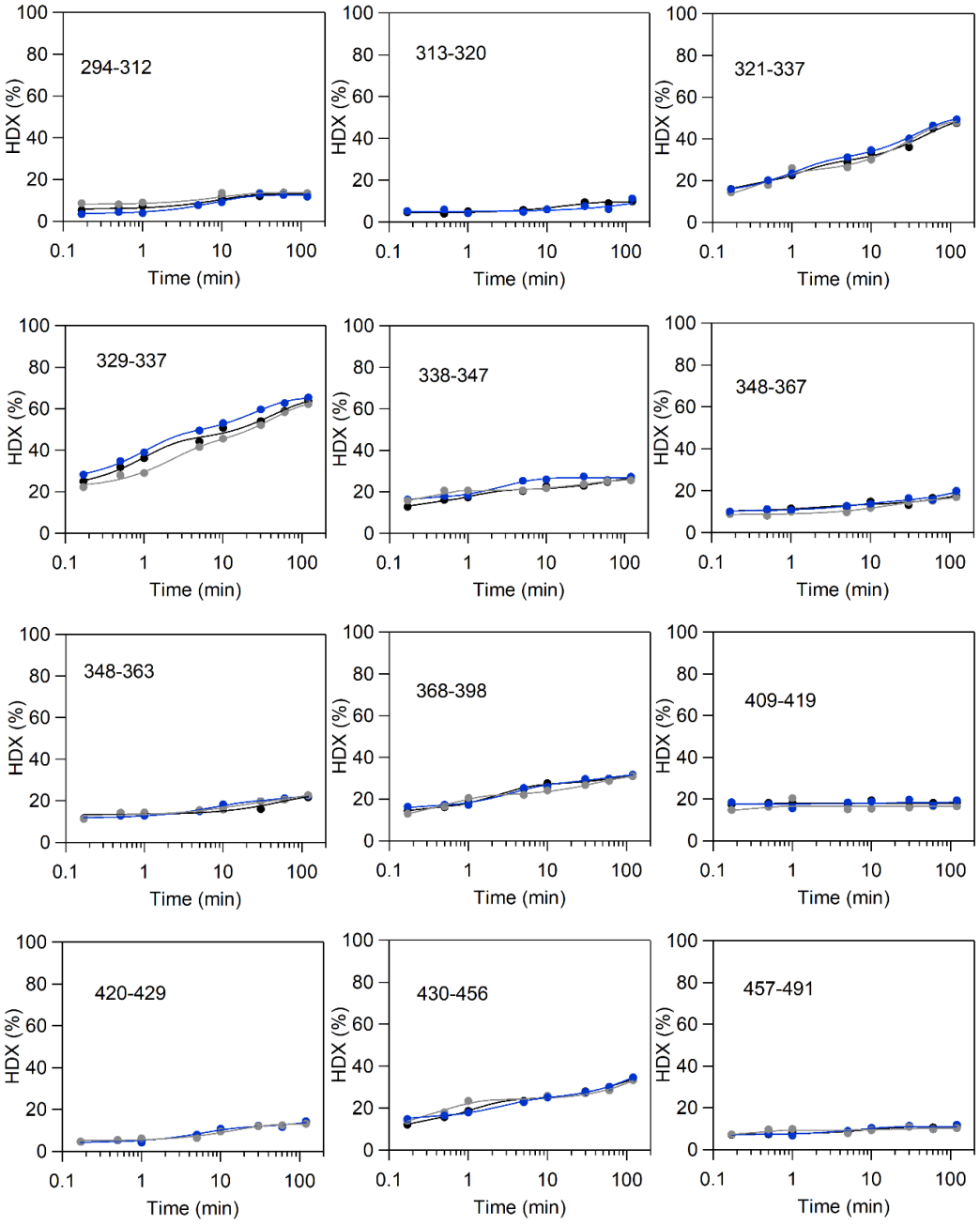
294-312
313-320
321-337
329-337
338-347
348-367
348-363
368-398
409-419
420-429
430-456
457-491
HDX (%)
Time (min)
0
20
40
60
80
100
0.1
1
10
100

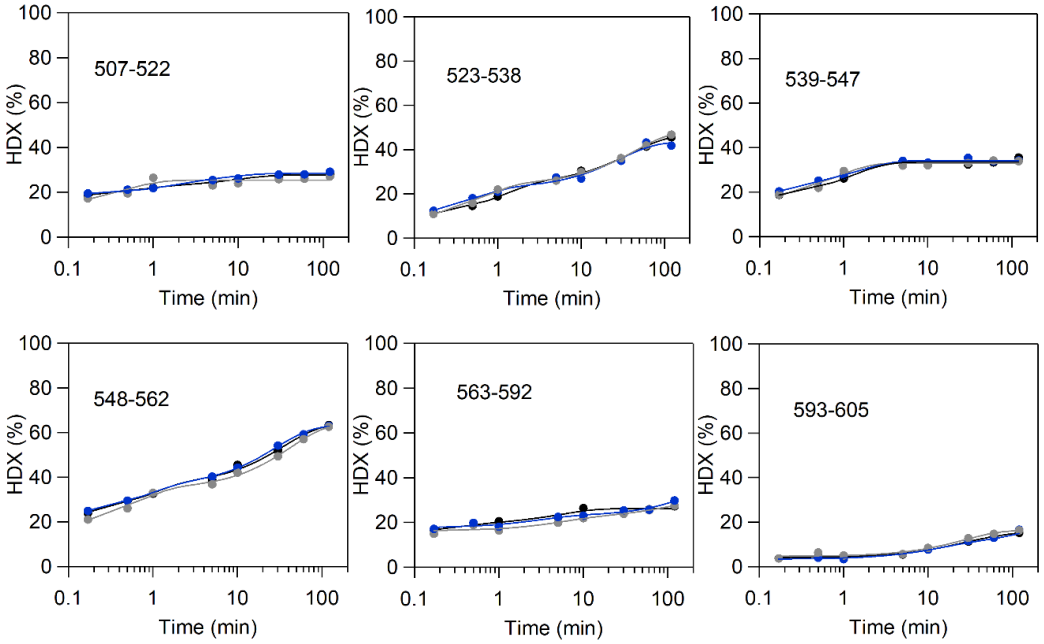
507-522
523-538
539-547
548-562
563-592
593-605
HDX (%)
Time (min)
0
20
40
60
80
100
0.1
1
10
100